Upper critical fields and superconducting transition temperatures of some zirconium-base amorphous transition-metal alloys

M. G. Karkut* and R. R. Hake

Department of Physics, Indiana University, Bloomington, Indiana 47405
(Received 13 December 1982; revised manuscript received 24 January 1983)

Superconducting upper critical fields $H_{c2}(T)$, transition temperatures T_c, and normal-state electrical resistivities ρ_n have been measured in the amorphous transition-metal alloy series $Zr_{1-x}Co_x$, $Zr_{1-x}Ni_x$, $(Zr_{1-x}Ti_x)_{0.78}Ni_{0.22}$, and $(Zr_{1-x}Nb_x)_{0.78}Ni_{0.22}$. Structural integrity of these melt-spun alloys is indicated by x-ray, density, bend-ductility, normal-state electrical resistivity, superconducting transition width, and mixed-state flux-pinning measurements. The specimens display $T_c = 2.1-3.8$ K, $\rho_n = 159-190$ $\mu\Omega$ cm, and $|(dH_{c2}/dT)_{T_c}| = 28-36$ kG/K. These imply electron mean free paths $l \approx 2-6$ Å, zero-temperature Ginzburg-Landau coherence distances $\xi_{G0} \approx 50-70$ Å, penetration depths $\lambda_{G0} \approx (7-10) \times 10^3$ Å, and extremely high dirtiness parameters $\xi_0/l \approx 300-1300$. All alloys display $H_{c2}(T)$ curves with *negative* curvature and (with two exceptions) fair agreement with the standard dirty-limit theory of Werthamer, Helfand, Hohenberg, and Maki (WHHM) for physically reasonable values of spin-orbit-coupling induced, electron-spin-flip scattering time τ_{so}. This is in contrast to the anomalously elevated $H_{c2}(T)$ behavior which is nearly linear in T that is observed by some, and the unphysically low-τ_{so} fits to WHHM theory obtained by others, for various amorphous alloys. Current ideas that such anomalies may be due to alloy inhomogeneity are supported by present results on two specimens for which relatively low-τ_{so} fits of $H_{c2}(T)$ to WHHM theory are coupled with superconductive evidence for inhomogeneity: relatively broad transitions at T_c and H_{c2}, current-density-dependent transitions at H_{c2}, and (in one specimen) a J-dependent, high-$H (>H_{c2})$, resistive "beak effect." In the $Zr_{1-x}Co_x$ and $Zr_{1-x}Ni_x$ series, T_c decreases linearly with x (and with unfilled-shell average electron-to-atom ratio $\langle e/a \rangle$ in the range $5.05 \leq \langle e/a \rangle \leq 6.40$) in fair agreement with previous results for these systems and contrary to the T_c vs $\langle e/a \rangle$ behavior of both amorphous and crystalline transition-metal alloys formed between near neighbors in the Periodic Table. Upper-critical-field and normal-state electrical resistivity measurements suggest that the molar electronic specific-heat coefficient γ_m decreases with x in parallel with T_c in the $Zr_{1-x}Co_x$ and $Zr_{1-x}Ni_x$ series. In the equal-$\langle e/a \rangle$ $(Zr_{1-x}Ti_x)_{0.78}Ni_{0.22}$ system, T_c decreases with x; in the $(Zr_{1-x}Nb_x)_{0.78}Ni_{0.22}$ system, T_c first increases and then decreases with x (hence with $\langle e/a \rangle$). These diverse $\langle e/a \rangle$ dependencies of T_c appear consistent with the ultraviolet-photoemission-spectroscopy indicated split-band model of such amorphous transition-metal alloys and the associated idea that the alloying dependence of T_c cannot be described by general T_c vs $\langle e/a \rangle$ rules.

I. INTRODUCTION

Despite their technological promise,[1] the electronic,[2,3] superconducting,[4-6] and magnetic[7] behavior of amorphous metals and alloys is not well understood. From the research standpoint it is of particular interest to examine transition metals in the extreme "dirty" limit of amorphous atomic disorder. Here the destruction of translational symmetry, although negating much of standard theory, might act to simplify some properties by suppressing fine structure in the electronic and vibrational spectra. Such smoothing could lead to general, albeit possibly unusual, behavior (e.g., the Mooij correlation,[8] the Collver-Hammond superconducting transition-temperature peak[9,10]) thus allowing greater eventual insight into the nature of d-electron metallic behavior.

Added impetus to the study of amorphous transition metals has been generated by the increasing availability of bulk specimens, kinetically (if not thermodynamically) stable at room temperature. These can now be obtained as "metallic glasses," quenched from the liquid at about 10^6 K/sec by various melt-spinning or melt-splatting techniques.[11] Unfortunately, the measurements of different lab-

oratories on independently produced metallic glasses are not always in good agreement, evidently due to the sensitivity of some measured properties to details of the quenching and fabrication procedures.

One area of such disagreement has arisen in the determination of the temperature dependence of the upper critical fields $H_{c2}(T)$ of amorphous transition-metal (TM) superconductors. For many years there have been reports in the literature[12-19] that their $H_{c2}(T)$ curves displayed an unusual linearity in T. However, most of these measurements were made at relatively high reduced temperatures $t \equiv T/T_c > \sim 0.6$ where near linearity might be expected. On the other hand, one investigation which allowed a meaningful comparison with theory, that of Togano and Tachikawa[20] on amorphous $Zr_{0.77}Rh_{0.23}$ down to $t = 0.4$, showed negative curvature in $H_{c2}(T)$, in fair accordance with the standard weak coupling, "dirty-limit" theory of Werthamer, Helfand, and Hohenberg[21] and Maki[22] (WHHM).

More recently, several groups[23-25] have reported dramatically enhanced $H_{c2}(T)$ that is nearly linear in T down to reduced temperatures as low as 0.2 ["Tenhover linearity"[23] (TL)], while others[26-31] observe nonenhanced behavior that has negative curvature in T more like that predicted by the WHHM theory. Tenhover et al. suggested[23] that TL in glassy TM was associated with precursor electron localization in their high normal-state electrical resistivity $\rho_n = 120-180$ $\mu\Omega$ cm specimens, where the electron mean free path l approximates interatomic distances (the Ioffe-Regel[32] condition). Despite some transport-property evidence[33-36] for very weak precursor-electron-localization effects in high-ρ_n bulk alloys, the association[23] of TL with high-ρ_n-indicated precursor electron localization would appear questionable, since WHHM theory is in fair agreement with $H_{c2}(T)$ curves measured for disordered crystalline TM alloys with $\rho_n = 100-150$ $\mu\Omega$ cm.[37-39] In addition, Carter et al.[27] observed TL in amorphous $Mo_{0.78}Ge_{0.22}$ in which transmission electron microscopy disclosed (50–200)-Å bcc crystallites and absence of TL in more homogeneous specimens. They were thus led to suggest that inhomogeneities on the order of the zero-temperature Ginzburg-Landau coherence length ($\xi_{G0} \approx 30-100$ Å in dirty alloys) could be responsible for TL. Such fine-scale inhomogeneity might not be apparent in ordinary x-ray diffraction studies, nor would it produce broadening of the superconducting transition in zero applied magnetic field since $\xi_G(T)$ $= \xi_{G0}[1-(T/T_c)]^{-1/2}$ becomes so large near T_c that spatial averaging would occur over regions much larger than the inhomogeneity scale. More recently, other investigators[31,40,41] have adduced various types of evidence in support of the above inho-

mogeneity interpretation,[27] but detailed understanding of $H_{c2}(T)$ behavior in amorphous TM alloy superconductors has not yet been achieved.

In this paper,[42] an extension of earlier work,[28,43] we report studies of the upper critical fields $H_{c2}(T)$ and superconducting transition temperatures T_c in four Zr-base, metallic-glass alloy series: $Zr_{1-x}Co_x$, $Zr_{1-x}Ni_x$, $(Zr_{1-x}Ti_x)_{0.78}Ni_{0.22}$, and $(Zr_{1-x}Nb_x)_{0.78}Ni_{0.22}$. Since the above history would suggest the sensitivity of such properties to fabrication techniques, we report melt-spinning procedures and structure-related studies (x-ray, density, normal-state electrical resistivity, superconducting transition width, flux-pinning, and flux-flow characteristics) in some detail, and compare where possible our results with those of others on amorphous alloys made independently in other laboratories. In a planned subsequent paper[36] we shall report the extension of earlier studies[33-35] of anomalous normal-state electrical resistance behavior (negative temperature coefficients of resistivity and negative magnetoresistance) in these and other high-ρ_n glassy and crystalline TM alloys.

II. SPECIMEN FABRICATION AND CHARACTERIZATION

A. Fabrication

Table I lists some structural properties of the amorphous alloys of the present study. Table I, column 1 shows the compositions of the 18 specimens. These are all of the so-called "early-late" TM alloy class, commonly designated $T_E T_L$. Such alloys were first reported by Ray et al.[44] and are of particular research interest because (a) their various properties may be studied over wide concentration ranges (Table I, columns 1 and 2) in contrast to TM metalloid glasses, and (b) they do not require stabilization by metalloids, so that some complication in electronic and structural conditions is avoided.

Table II lists some properties of the starting materials. These were consolidated by melting etched and weighed amounts in a laboratory arc furnace utilizing a Zr-gettered argon atmosphere, a water-cooled copper hearth, and a tungsten electrode. Each button (3–30 g) was turned over and remelted at least five times to promote homogeneity. Weight loss during melting was in all cases small enough that alloy compositions could be adequately determined from the weights of materials melted.

Figure 1 shows a schematic of the melt-spinning device, similar to that described by Liebermann and Graham.[50] After arc melting, the usually brittle buttons were broken into fragments, etched to remove surface contamination, and then placed in the

TABLE I. Some structure-related properties of amorphous Zr-base alloys.

Alloy specimen[a] (1)	$\langle e/a \rangle$[b] (2)	$2\theta_1$[c] (deg) (3)	Q_p[d] (Å⁻¹) (4)	$\langle R_g \rangle$[e] (Å) (5)	Structure[f] (6)	$\langle M \rangle$[g] (g/mol) (7)	$[\rho_n(4.2\text{ K})/\rho(300\text{ K})]$[h] (8)	ΔT^i (T_c) (mK) (9)	D^j (g/cm³) (10)	V_0^k (Å³/atom) (11)	η_a^l (12)	$(\eta_a/\eta_c)^m$ (13)
$Zr_{0.79}Co_{0.21}$ no. 2	5.05	35.9	2.512	1.527	$a(e)$	84.44	1.048	10	6.68	20.99	0.728	0.983
$Zr_{0.75}Co_{0.25}$ no. 1	5.25	36.0	2.518	1.513	$a(e)$	83.15	1.045	8	6.86	20.13	0.741	1.001
$Zr_{0.72}Co_{0.28}$ no. 1	5.40	36.2	2.532	1.502	$a(e)$	82.18	1.065	12	6.88	19.83	0.738	0.998
$Zr_{0.65}Co_{0.35}$ no. 2	5.75	36.8	2.572	1.478	$a(e)$	79.92	1.059	14	7.05	18.82	0.745	1.006
$Zr_{0.62}Co_{0.38}$ no. 1[n]	5.90	37.0	2.586	1.467	$a+c(4)$	78.95	1.055	4	7.20	18.21	0.755	1.020
$Zr_{0.78}Ni_{0.22}$ no. 3	5.32	35.8	2.505	1.521	$a(e)$	84.07	1.082	12	6.78	20.58	0.736	0.994
$Zr_{0.76}Ni_{0.24}$ no. 2	5.44	35.9	2.512	1.514	$a(e)$	83.42	1.046	17	6.87	20.16	0.742	1.002
$Zr_{0.73}Ni_{0.27}$ no. 1	5.62	36.0	2.518	1.503	$a(e)$	82.44	1.062	43	6.88	19.90	0.738	0.997
$Zr_{0.70}Ni_{0.30}$ no. 2[n]	5.80	36.4	2.545	1.492	a	81.47	1.058	16	7.04	19.22	0.750	1.013
$Zr_{0.635}Ni_{0.365}$ no. 1[n]	6.19	37.0	2.586	1.469	$a+c(2)$	79.35	1.059	8	7.12	18.51	0.746	1.008
$Zr_{0.60}Ni_{0.40}$ no. 1[n]	6.40	37.4	2.613	1.456	$a+c(4)$	78.22	1.053	39	7.24	17.94	0.752	1.016
$(Zr_{0.9}Ti_{0.1})_{0.78}Ni_{0.22}$ no. 1	5.32	36.1	2.525	1.511	$a(e)$	80.69	1.072	8	6.65	20.15	0.736	0.995
$(Zr_{0.8}Ti_{0.2})_{0.78}Ni_{0.22}$ no. 1	5.32	36.4	2.545	1.501	$a(e)$	77.31	1.057	10	6.55	19.60	0.742	1.002
$(Zr_{0.7}Ti_{0.3})_{0.78}Ni_{0.22}$ no. 1	5.32	36.8	2.572	1.490	$a(e)$	73.93	1.073	6	6.42	19.12	0.745	1.006
$(Zr_{0.95}Nb_{0.5})_{0.78}Ni_{0.22}$ no. 1	5.359	36.0	2.518	1.515	$a(e)$	84.13	1.052	16	6.84	20.43	0.733	0.991
$(Zr_{0.90}Nb_{0.10})_{0.78}Ni_{0.22}$ no. 1	5.398	36.2	2.532	1.510	$a(e)$	84.20	1.077	50	6.94	20.15	0.735	0.994
$(Zr_{0.85}Nb_{0.15})_{0.78}Ni_{0.22}$ no. 1	5.437	36.4	2.545	1.504	$a(e)$	84.27	1.040	74	7.04	19.88	0.737	0.997
$(Zr_{0.80}Nb_{0.20})_{0.78}Ni_{0.22}$ no. 1	5.476	36.8	2.572	1.499	$a(e)$	84.33	1.041	140	7.05	19.86	0.730	0.986

[a]Nominal compositions in atomic fractions.

[b]Average electrons per atom outside closed shells of the free atoms.

[c]Angular position of first peak in the x-ray diffraction pattern for copper $K\alpha$ radiation ($\lambda = 1.542$ Å).

[d]Scattering vector at first peak in the x-ray diffraction pattern, $Q_p = 4\pi(\sin\theta_1)/\lambda$.

[e]Average Goldschmidt radius (12-fold coordination). For alloy $A_{1-x}B_x$, $\langle R_G \rangle = (1-x)R_{GA} + xR_{GB}$, where R_{GA} and R_{GB} are the Goldschmidt radii for elements A and B from Ref. 45.

[f]$a \equiv 100\%$ amorphous to within resolution of x-ray scan; (e), etched; $a+c(n)$, amorphous but with n discernible crystalline spikes.

[g]Average atomic mass. Elemental values from Ref. 46.

[h]Normal-state resistivity ratio. At 4.2 K, high magnetic fields were applied to quench above-T_c superconductivity in higher-T_c specimens as discussed in the text.

[i]Zero-H transition breadths as discussed in the text.

[j]Density, determined by Archimedes method ($\pm 0.75\%$), Ref. 47.

[k]Average atomic volume $V_0 = \langle M \rangle/(DN_A)$, where N_A is Avogadro's number.

[l]Amorphous alloy packing fraction $\eta_a = (4\pi/3)\langle R_G^3 \rangle/V_0$.

[m]Ratio of amorphous to ideal crystalline close-packed ($\eta_c = 0.740$) packing fractions.

[n]Specimens previously reported in Ref. 28.

TABLE II. Some properties of the starting materials.

Metal (1)	Supplier (2)	Grade[a] (3)	Nominal purity[a] (%) (4)	M[b] (g/mol) (5)	Common structure[b] (6)	V_0[c] (Å^3/atom) (7)	R_G[d] (Å) (8)	η[e] (9)	γ_m[f] (mJ/mol K^2) (10)
Ti	MRC[g]	"VP"	99.9	47.90	hcp	17.66[i]	1.47	0.753	3.41
Co	CCC[h]		98—99	58.93	hcp	11.11[j]	1.25	0.736	4.73
Ni	MRC	"VP"	99.99	58.71	fcc	10.95[j]	1.24	0.729	7.30
Zr	MRC	"VP"	99.9	91.22	hcp	23.28[j]	1.60	0.737	2.91
Nb	MRC	"VP"	99.96	92.91	bcc	17.98[j]	1.46	0.725	7.66

[a]As specified by supplier.
[b]Atomic mass from Ref. 46.
[c]Atomic volume.
[d]Goldschmidt radius from Ref. 45.
[e]Packing fraction $(4\pi/3)R_G^3/V_0$.
[f]Molar electronic specific-heat coefficient from Ref. 48.
[g]Materials Research Corporation, Orangeburg, New York.
[h]City Chemical Corporation, New York, New York.
[i]Reference 49 (the value given in Ref. 48 is incorrect for hcp Ti).
[j]Calculated from atomic volumes in units cm^3/mol given in Ref. 48.

quartz tube of an induction melter as shown in Fig. 1. The tube was flushed with inert gas, rf power was applied to the surrounding coil so as to melt the alloy, and then an inert-gas overpressure of ~ 8 psi (gauge) was applied, forcing a molten jet through the (0.4—0.5)-mm-diam orifice in the hemispherical bottom end of the quartz tube. The jet impinged upon the circumferential surface (about 1—2 mm from the quartz-tube orifice) of the 8.8-cm-diam copper wheel rotating at 4500—9200 rpm. The wheel surface was polished just prior to melt spinning with fine emery paper (followed by methanol cleaning) so as to remove the oxide layer and promote thermal contact between melt pool and the wheel. The high-velocity (1.3—2.6 km/min) ribbon was ducted through a copper catching tube into a sealed bell jar where it spiraled to a halt. The entire apparatus was operated in a flowing helium atmosphere so as to re-

tard oxide layer formation, promote ribbon quality,[51] and prevent ignition of the pyrophoric Zr alloys. Ribbons were generally continuous and reasonably uniform in cross section ($\sim 25-35$ μm thickness, ~ 1 mm width). The ribbons displayed a shiny top surface which had been less rapidly quenched than the relatively dull bottom surface, since the latter had been in direct contact with the copper disk. Most ribbons could be bent 180° without fracture[51,52] (the so-called[53] "bend-ductility test").

B. X-ray diffraction

Sections of all ribbons were examined by x-ray diffraction, first using the Debye-Scherrer transmission technique with Ni-filtered copper $K\alpha$ radiation. Ribbons which displayed only the typical amorphous-structure diffuse halos with no sharp crystalline lines were then subjected to more sensitive and accurate reflection diffractometry. The Phillips scanning diffractometer, equipped with a scintillation-detector counter and a carbon-crystal diffracted-beam monochromator, displayed excellent resolution and angular accuracy on test scans of a Si-powder standard. About twelve 2.5-cm-long strips were cut from the ribbon and placed side by side and shiny side up on a microscope slide, which was then fastened to the specimen plate of the diffractometer. All such strip arrays were scanned through scattering angles $10° \leq 2\theta \leq 100°$ using an angular speed of 1 deg/min, detector time constant $\tau = 2$ sec,[54] and copper $K\alpha$ radiation.
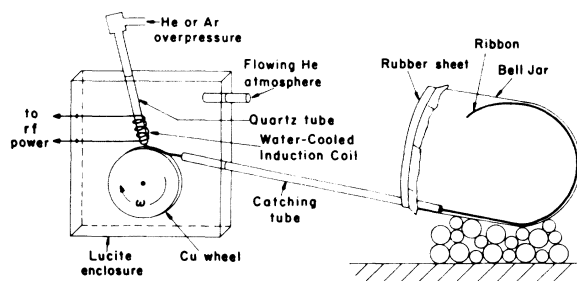
FIG. 1. Schematic diagram of the melt-spinning apparatus as discussed in the text. A two-size DRPHS model supports the bell jar.

Figure 2 shows a scan for an etched array of $Zr_{0.73}Ni_{0.27}$ strips. The scan is typical of those alloys designated (Table I, column 6) a or $a(e)$ [a, amorphous to within resolution of the x-ray scan; (e), chemically etched array] in showing the usual amorphous-structure broad peaks with primary $2\theta_1$ (Table I, column 3) and secondary $2\theta_2$ maxima. Sharp spikes which sometimes were superimposed upon the two-broad-peak amorphous background were usually due to reflection from crystalline inclusions on the shiny, less rapidly quenched, top ribbon surface since (a) no evidence for crystallinity had appeared in the volume-averaging transmission Debye-Scherrer photographs, (b) spikes usually disappeared on dull-side-up diffractometer scans, (c) mechanical polishing or chemical etching so as to remove 2—7 μm of the shiny surface usually resulted in absence of spikes in subsequent scans.[28] Similar observations have been reported by Rapp and co-workers.[55,56] Etched specimens for the upper-critical-field and normal-state electrical resistivity measurements were normally taken from the arrays which had been subjected to diffractometry. Some specimens designated (Table I, column 6) a or $a+c(n)$ (amorphous but with n discernible crystalline spikes) were measured in the unetched condition. As previously reported[28] (apparent surface) crystalline inclusions appear to have little effect on the reduced upper-critical-field curves $h^*(t)$ (Sec. III). In the present work the insensitivity of $h^*(t)$ to etching is indicated in Fig. 12 which shows data for $Zr_{0.72}Co_{0.28}$ before and then after a top-surface etch which eliminated crystalline spikes from its diffractogram.

C. Density

The densities D of all amorphous alloys were determined by the Archimedes[47] method, weighing ribbon spools of about 0.5 g first in air and then in CCl_4 with a Mettler H31 balance. The density
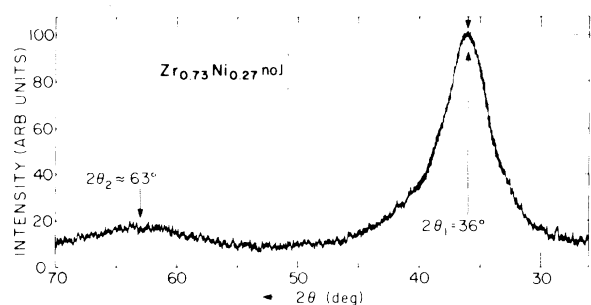
FIG. 2. X-ray diffractogram of amorphous $Zr_{0.73}Ni_{0.27}$ no. 1, as discussed in the text. The radiation is $Cu K\alpha$ with $\lambda = 1.542$ Å.

values (Table I, column 10) were used to reduce geometric uncertainty[28,34,57] in normal-state electrical resistivity determinations (Table III, column 5), and to calculate average atomic volumes V_0 (Table I, column 11) and amorphous-alloy packing fractions η_a (Table I, column 12). The latter are all within 2% (Table I, column 13) of the ideal close-packed (fcc or hcp) crystalline value $\eta_c = 0.740$, about 16% higher than predicted by unrelaxed single-size dense random packing of hard-spheres (DRPHS) models,[58] and about 6% higher than obtained by Johnson and Williams[59] for non-$T_E T_L$ amorphous $Mo_{0.6}Ru_{0.4}$ by extrapolation to zero metalloid content. Present density data are in good agreement with those of Dong et al.,[60] but present measurements lie 4% above the determinations of Waseda and Chen[61] on amorphous $Zr_{0.70}Co_{0.30}$ and $Zr_{0.70}Ni_{0.30}$. Atomic volume versus alloy concentration plots[42] show small negative deviations from "Zen's law"[62] as previously observed for amorphous $Zr_{1-x}Ni_x$ alloys,[60] and suggestive of some degree of chemical short-range order.

D. Electrical resistivity

Table III lists various measured and calculated[63] electronic and superconducting properties of the present specimens. Measured helium-temperature normal-state electrical resistivities $\rho_n(4.2$ K) (Table III, column 5) for the present amorphous alloys are all very high[64,65] (159—190 $\mu\Omega$ cm) in comparison with most (but not all[8,33,35−39,66]) crystalline TM alloys. Meaningful comparison of metallic glass absolute resistivities measured in different laboratories is hindered by experimental uncertainties associated with thin-strip geometric measurements. In the present work a $\pm 7\%$ uncertainty in ρ_n was achieved by calculating specimen cross-sectional areas from measured alloy density,[28,34,57] and specimen length and mass. The latter (2—5 mg) was measured for each specimen with a Cahn electrobalance model 25. Our results for $Zr_{1-x}Ni_x$ (168—190 $\mu\Omega$ cm) are in reasonable agreement with those of Babić et al.[67] (164—182 $\mu\Omega$ cm) on a similar amorphous $Zr_{1-x}Ni_x$ series, and lower than the ~ 320 $\mu\Omega$ cm ($x = 0.24, 0.36$) upper limits reported by Buschow and Beekmans.[68] For $Zr_{1-x}Co_x$ our values (170—181 $\mu\Omega$ cm) can be compared only with isolated single-alloy measurements: 145 $\mu\Omega$ cm ($x = 0.3$)[24] and 190 $\mu\Omega$ cm ($x = 0.3$).[69]

Resistivity ratios $r \equiv \rho_n(4.2$ K$)/\rho(300$ K) (Table I, column 8) are not subject to the geometric error. We previously reported[57] good agreement for r on Allied Corporation Metglas® Fe-base amorphous alloys measured by Rayne and Levy[70] and ourselves.[57] However, for nonferromagnetic or nonantiferromag-

TABLE III. Some superconducting and electronic properties of amorphous Zr-based alloys.

Alloy specimen[a] (1)	T_c[b] (K) (2)	$(-dH_{c2}/dT)_{T_c}$[c] (kG/K) (3)	α[d] (4)	ρ_n[e] (4.2 K) ($\mu\Omega$ cm) (5)	γ_v[f] (10^3 erg/cm^3 K^2) (6)	γ_m[g] (mJ/mol K^2) (7)	N_γ[h] (states/eV atom) (8)	κ_1[i] (9)	ξ_{G0}[j] (Å) (10)	λ_{so}[k] (11)	τ_{so}[k] $\times 10^{14}$ (sec) (12)	τ_{tr}[m] $\times 10^{16}$ (sec) (13)	(τ_{so}/τ_{tr}) (14)	l[n] (Å) (15)	(ξ_0/l)[o] $\times 10^{-2}$ (16)
Zr$_{0.79}$Co$_{0.21}$ no. 2	3.78	34.1	1.82	170	4.55	5.75	1.22	86	50	3.5	12	11	110	3	3.3
Zr$_{0.75}$Co$_{0.25}$ no. 1	3.47	33.9	1.81	179	4.30	5.21	1.10	88	52	4	12	9	130	3	4.5
Zr$_{0.72}$Co$_{0.28}$ no. 1	3.12	33.8	1.80	181	4.23	5.06	1.07	88	55	4	13	8	160	3	5.4
Zr$_{0.65}$Co$_{0.35}$ no. 2	2.48	34.8	1.85	180	4.38	4.96	1.05	89	61	6	11	7	150	3	7.7
Zr$_{0.62}$Co$_{0.38}$ no. 1[p]	2.10	33.0	1.76	173	4.33	4.75	1.01	85	68			7		3	9.5
Zr$_{0.78}$Ni$_{0.22}$ no. 3	3.47	31.9	1.70	168	4.30	5.33	1.13	83	54	3	16	10	160	3	4.2
Zr$_{0.76}$Ni$_{0.24}$ no. 2	3.29	31.5	1.68	178	4.01	4.87	1.03	85	55	3	16	8	200	3	5.3
Zr$_{0.73}$Ni$_{0.27}$ no. 1	3.10	31.9	1.70	178	4.06	4.87	1.03	85	57	3	17	8	230	3	5.9
Zr$_{0.70}$Ni$_{0.30}$ no. 2[p]	3.00	31.3	1.67	178	3.99	4.62	0.98	84	58	5	11	7	160	3	6.8
Zr$_{0.635}$Ni$_{0.365}$ no. 1[p]	2.39	33.3	1.77	190	3.98	4.43	0.94	90	63	2	34	5	610	2	10.4
Zr$_{0.60}$Ni$_{0.40}$ no. 1[p]	2.15	30.0	1.60	182	3.74	4.04	0.86	84	70			5		2	12.9
(Zr$_{0.9}$Ti$_{0.1}$)$_{0.78}$Ni$_{0.22}$ no. 1	3.32	32.9	1.75	180	4.15	5.03	1.07	87	54	3	16	8	190	3	5.0
(Zr$_{0.8}$Ti$_{0.2}$)$_{0.78}$Ni$_{0.22}$ no. 1	3.09	35.2	1.87	172	4.64	5.48	1.16	88	54	2	26	9	280	3	4.7
(Zr$_{0.7}$Ti$_{0.3}$)$_{0.78}$Ni$_{0.22}$ no. 1	2.78	36.3	1.94	182	4.53	5.21	1.10	92	56	3	19	8	230	3	5.9
(Zr$_{0.95}$Nb$_{0.05}$)$_{0.78}$Ni$_{0.22}$ no. 1	3.65	31.5	1.68	171	4.18	5.14	1.09	83	53	3	15	9	170	3	4.2
(Zr$_{0.90}$Nb$_{0.10}$)$_{0.78}$Ni$_{0.22}$ no. 1	3.65	30.1	1.61	167	4.09	4.96	1.05	80	54	3	15	9	170	3	4.3
(Z$_{0.85}$Nb$_{0.15}$)$_{0.78}$Ni$_{0.22}$ no. 1	3.56	29.5	1.57	159	4.21	5.04	1.07	77	55	7?	6?	9	70?	3	4.2
(Zr$_{0.8}$Nb$_{0.20}$)$_{0.78}$Ni$_{0.22}$ no. 1	3.34	28.2	1.50	162	3.94	4.71	1.00	76	58	10?	5?	8	60?	3	5.0

[a] Nominal compositions in atomic fractions.

[b] Superconducting transition temperature by extrapolation of $H_{c2}(T)$ curves to zero field.

[c] Limiting upper-critical-field slope at T_c (experimental uncertainty ±2%).

[d] Maki paramagnetic limitation parameter $\alpha = 5.33 \times 10^{-2}(-dH_{c2}/dT)_{T_c}$ where the slope is in kG/K (Ref. 39).

[e] Normal-state electrical resistivity at 4.2 K, accurate to about ±7% due to geometric uncertainty as discussed in the text.

[f] Electronic specific-heat coefficient per unit volume, calculated from $(dH_{c2}/dT)_{T_c}$ and ρ_n in accordance with Eq. (2) with experimental uncertainty ±9%.

[g] Electronic specific-heat coefficient per mole, calculated from γ_v and density-determined atomic volume V_0 with experimental uncertainty ±10%.

[h] Dressed one-spin-state density at the Fermi level calculated from γ_m in accordance with Eq. (3) (experimental uncertainty ±10%).

[i] Ginzburg-Landau extrinsic $\kappa_1 \simeq 7500 \rho_n \gamma_v^{1/2}$ where ρ_n is in Ω cm and γ_v is in erg cm^{-3} K^{-2} (Ref. 39).

[j] Ginzburg-Landau coherence distance at $T=0$, $\xi_{G0} \simeq 0.85(\xi_0 l)^{1/2} = 0.85 \times 10^{-6}(\rho_n \gamma_v T_c)^{-1/2}$, where ρ_n and γ_v are in units specified in footnote i (Ref. 39).

[k] Spin-orbit-coupling induced spin-flip scattering parameter determined by fit of WHHM theory to $h*$ vs t data as discussed in the text. Only the best-fit λ_{so} for the relatively low-t data is specified.

[l] Spin-orbit scattering time $\tau_{so} = 2\hbar(3\pi k_B T_c \lambda_{so})^{-1} = 16.2 \times 10^{-13} (T_c \lambda_{so})^{-1}$ (Refs. 39 and 103).

[m] Transport scattering time $\tau_{tr} = 2.21 \times 10^8 \gamma_v [\rho_n n^{4/3}(S/S_f)^2]^{-1}$ where units are as in footnote i (Ref. 39). The approximation used for the conduction-electron density n and the Fermi-surface ratio (S/S_f) are discussed in the text.

[n] Electron mean free path $l = 1.27 \times 10^4 [\rho_n n^{2/3}(S/S_f)]^{-1}$ cm, where ρ_n is in Ω cm and n and S/S_f are discussed in the text (Ref. 39).

[o] Dirtiness parameter $\xi_0/l = 1.38 \times 10^{-12}(\tau_{tr}T_c)^{-1}$ (Ref. 39).

[p] Specimens previously reported in Ref. 28. ρ_n and γ_v values have been slightly revised in accordance with the present more accurate specimen mass measurements used to determine the ρ_n geometrical factor.

netic high-ρ_n crystalline[71] and amorphous[24,72] alloys, fluctuation and/or remnant superconductivity usually combine with the normal-state negative-temperature coefficient of resistivity to produce a peak in $\rho(T,H=0)$ at about $2T_c$.[73,74] For the higher-T_c alloys of the present study, we found it necessary to apply high magnetic fields at 4.2 K so as to quench above-T_c superconductivity and thus allow measurement of the normal state $\rho_n(4.2$ K). Because these complications are either ignored or treated differently by other workers, it is currently difficult to make meaningful r comparisons on superconducting amorphous alloys measured in different laboratories. The present resistivity ratios (Table I, column 8) $r=1.040-1.082$ imply *average* temperature coefficients of resistivity over the range $\Delta T=300-4$ K of

$$\langle \alpha \rangle \equiv \rho^{-1}(\Delta\rho/\Delta T) \approx 0.06(300 \text{ K})^{-1}$$

$$= -2\times 10^{-4} \text{ K}^{-1} ,$$

of somewhat larger magnitude than the high temperature

$$\alpha(300-350 \text{ K}) \equiv \rho^{-1}(d\rho/dT) \approx -1\times 10^{-4} \text{ K}^{-1}$$

read from the α vs ρ_n graph of Mooij[8] for $\rho_n = 180$ $\mu\Omega$ cm (Table III, column 5). The α difference is consistent with previous work[36,75] on high-ρ_n crystalline TM alloys showing that the magnitude of the approximate $\alpha(2$ K) is larger than the $\alpha(T\approx 325$ K) values in the Mooij plot at similar ρ_n.

III. UPPER CRITICAL FIELDS

A. Experimental method

Upper critical fields were measured resistively using the standard dc four-point-contact method. The cryogenic and magnetic systems, as well as the electrical resistivity measuring apparatus and method are similar to those described earlier.[39,74] Data at

applied fields $H < \sim 25$ kG were normally obtained with a low-residual-field ($< \sim 10$ G) 30-kG Nb-Zr-wire superconducting solenoid[39]; while data at $H > \sim 10$ kG were obtained with a 140-kG Nb$_3$Sn-tape superconducting solenoid.[74] Field homogeneity of both magnets was better than $\pm 0.1\%$ over the specimen volumes. Electrical resistance measurements were made using separate probes for two orientations (see Fig. 3 inset): (1) the current density $\vec{J}$ (and the long axis of the specimen) parallel to $\vec{H}$, and (2) the current density $\vec{J}$ (and the long axis of the specimen) perpendicular to $\vec{H}$. In the latter orientation the specimen was held so that its wide flat surface was perpendicular to $\vec{H}$. Copper potential leads and indium-coated copper current contacts were held firmly and nondestructively against the thin-strip specimens by beryllium-copper-strip springs. Specimens were immersed directly in a liquid-helium bath contained by a stainless-steel Janis insert Dewar. Temperatures down to 1.1 K could be obtained by pumping over the helium bath.

For the critical-field measurements, temperatures were held constant to within ± 0.001 K and were determined with an absolute accuracy of about $\pm 1\%$ by measurement of the helium vapor pressure. Resistive voltages were recorded on the y axis of an xy recorder whose x axis was driven by a voltage nearly proportional to the applied magnetic field.

B. Resistive upper-critical-field transitions

Figures 3—5 show typical normalized resistance versus longitudinal ($\vec{J}||\vec{H}$) and perpendicular ($\vec{J}\perp\vec{H}$) applied field curves, similar in some respects to those reported[39,71,74,76-78] for high-ρ_n crystalline TM alloys using similar apparatus and techniques. Figure 3 shows how H_{c2} is arbitrarily defined (as in previous work[28,39]) as the intersection of the steep linear portion of the $\vec{H}||\vec{J}=3$ A/cm^2 curves with the $R=0$ axis. The definition of H_{c2} as
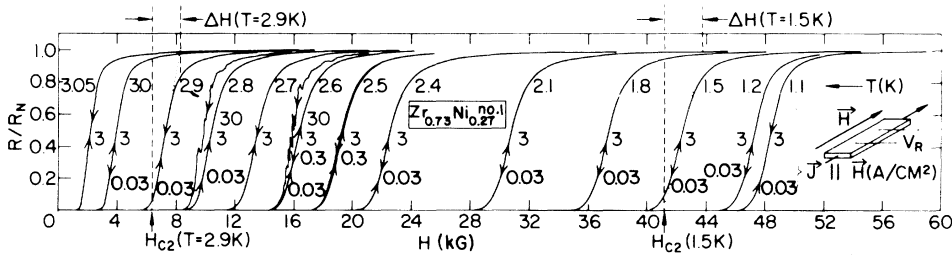
FIG. 3. X-Y recorder tracings of normalized resistance R/R_N (R_N, normal-state resistance) vs longitudinal applied magnetic field H for amorphous Zr$_{0.73}$Ni$_{0.27}$ no. 1. The curves at $T=1.5$ and 2.9 K show how the upper critical fields $H_{c2}(T)$ and the transition widths $\Delta H(T)$ are defined as discussed in the text. The arrows on the curves indicate the directions of the field sweeps. The inset at the right shows the geometrical relationships for the $\vec{J}||\vec{H}$ orientation. (V_R is the resistive voltage proportional to R.) For the $\vec{J}\perp\vec{H}$ orientation (Figs. 4 and 5) $\vec{H}$ is perpendicular to both $\vec{J}$ and the wide flat surface of the specimen.
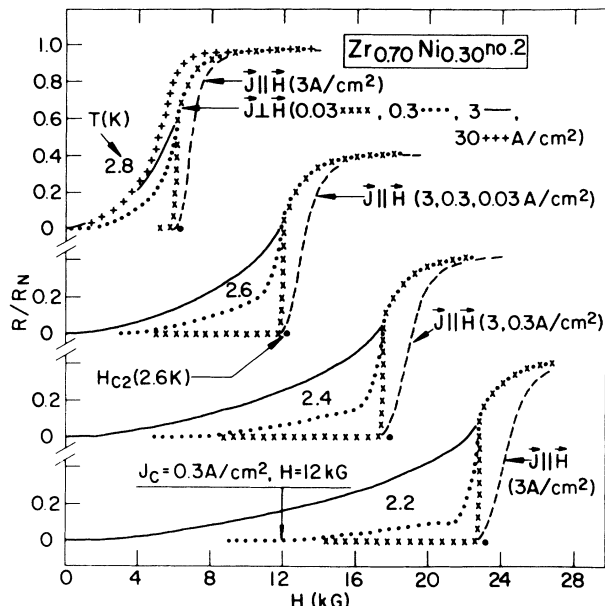
FIG. 4. Resistive transitions for amorphous $Zr_{0.70}Ni_{0.30}$ no. 2 as discussed in the text. The curve for $T=2.2$ K and $\vec{H}\perp\vec{J}=0.3$ A/cm^2 shows that the critical mixed-state depinning current density is $J_c=0.3$ A/cm^2 at $H=12$ kG as discussed in the text.
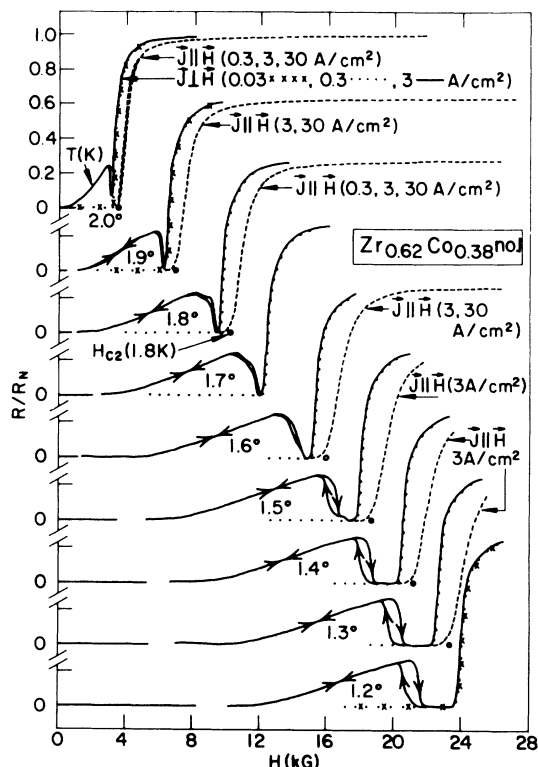
FIG. 5. Resistive transitions for amorphous $Zr_{0.62}Co_{0.38}$ no. 1 as discussed in the text.

the transition midpoint at $J=3$ A/cm^2 would have negligible effect[28] on the shapes of the $H_{c2}(T)$ (Figs. 7–9) or $h^*(t)$ (Figs. 11–16) curves. Several features of the $\vec{J}\,||\,\vec{H}$ curves are notable:

(1) The current-density (J) dependence at $0.03\leq J\leq 3$ A/cm^2 (usually indicative of filamentary or surface superconductivity[39,76–78]) is negligible. This contrasts with high-ρ_n crystalline alloys[39] in which surface superconductivity atypical of the bulk (not the ideal Saint-James–de Gennes sheath[79]) often produces J-dependent transitions above H_{c2}. Specimen heating evidently accounts for the elevation and instability of the $J=30$ A/cm^2 traces apparent in Figs. 3 and 4, since these effects are usually minimal (see Fig. 5) below the liquid-helium λ-point transition at $T=2.17$ K, where the bath thermal conductance increases drastically.

(2) A long high-field tail appears on the R/R_N vs H curves and restoration of full resistance occurs only over a very wide applied field range. For both high-ρ_n crystalline and amorphous alloys, positive slopes in R/R_N vs H can be observed[73,74] (at factors of 100 higher amplification than those of Figs. 3–5) up to about twice the zero-temperature upper critical field $H_{c2}(T=0)$ and have been associated[71,74,78,80] with fluctuation superconductivity.

(3) The *slope* of the R/R_N vs H curves in the relatively steep and nearly linear transition region decreases as temperature decreases below T_c. Figure 6
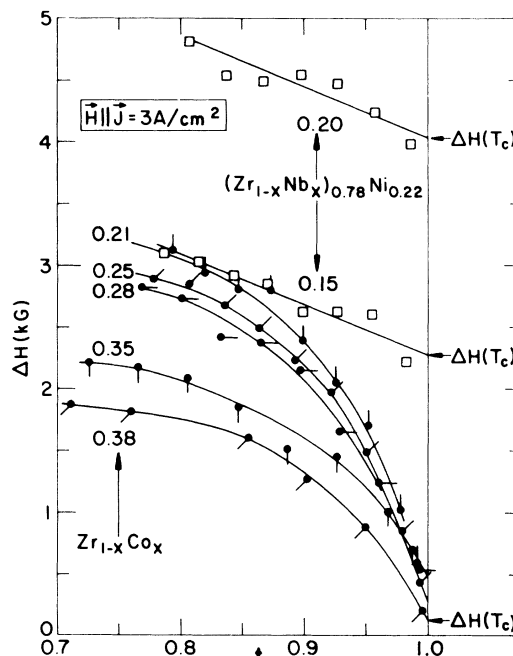
FIG. 6. Upper-critical-field transition widths $\Delta H(t)$, defined as shown in Fig. 3 vs reduced temperature $t\equiv T/T_c$ for various amorphous alloys, all for $\vec{H}\,||\,\vec{J}=3$ A/cm^2. $\Delta H(T_c)$ is obtained by extrapolation to $t=1.0$ as shown for three of the curves.

shows the transition breadth $\Delta H(T)$, defined as shown in Fig. 3, plotted versus reduced temperature $t \equiv T/T_c$ for $Zr_{1-x}Co_x$ alloys and for several $(Zr_{1-x}Nb_x)_{0.78}Ni_{0.22}$ alloys with exceptionally wide transitions as discussed below. The zero-H transition breadths at T_c, $\Delta T(T_c)$ are obtained by extrapolating $\Delta H(T)$ curves to T_c, as shown in Fig. 6, so as to obtain $\Delta H(T_c)$. One then obtains

$$\Delta T(T_c) = \frac{\Delta H(T_c)}{(-dH_{c2}/dT)_{T_c}} \,, \tag{1}$$

where $(dH_{c2}/dT)_{T_c}$ is the measured upper-critical-field slope (Table III, column 3). These *resistive* transition breadths $\Delta T(T_c) = 4-140$ mK (Table I, column 9), possibly less meaningful than *calorimetric* widths,[29,81] are presumably related to superconductive fluctuations and to the ratio of the inhomogeneity scale to the coherence length ξ_{G0}. The widths may be compared with those reported for amorphous alloys by other workers: 5 mK in $Zr_{0.75}Ni_{0.25}$,[31] less than 20 mK (one specimen at 40 mK) in $Zr_{1-x}Ni_x$,[67] less than 20 mK in $Zr_{1-x}Cu_x$,[29] 10–150 mK in $Zr_{1-x}Co_x$,[55] less than 50 mK in $Zr_{0.7}(T_L)_{0.3}$ $(T_L = Cu, Ni, Co)$,[24] 80 mK in sputtered $Nb_{0.75}Sn_{0.25}$,[82] less than 200 mK to greater than 1 K in Nb- and Ta-based alloys.[18] Unfortunately, these comparisons must be treated with reservation because the transition-width criteria vary somewhat and the J dependence, if any, is seldom reported.

Figures 4 and 5 compare typical resistive curves for the $\vec{J}||\vec{H}$ and $\vec{J}\perp\vec{H}$ orientations. Noteworthy features of the $\vec{J}\perp\vec{H}$ curves are the following:

(1) Above the steep resistive onset near H_{c2} there is negligible current-density J dependence for $0.03 \leq J \leq 3$ A/cm^2.

(2) A long high-field tail appears on the R/R_N vs H curves and restoration of full resistance occurs only over a very wide applied field range, as is the case in high-ρ_n crystalline alloys.[39,71,74,78] Here as for $\vec{J}||\vec{H}$, the long tail has been attributed to fluctuation superconductivity.[71,74,78,80]

(3) The *slope* of the R/R_N vs H curves in the relatively steep and nearly linear transition region shows little temperature dependence, in contrast to the $\vec{J}||\vec{H}$ case. This leads to a marked anisotropy in the low-T transition curves as shown in Figs. 4 and 5. Transitions near H_{c2} for $\vec{J}||\vec{H}$ are broader than those for $\vec{J}\perp\vec{H}$. In the transition regions the curves of Figs. 4 and 5 are very similar to those reported[83] for crystalline high-ρ_n $Ti_{0.84}Mo_{0.16}$, and ascribed to effective one dimensionality in the fluctuation spectrum for the $\vec{J}||\vec{H}$ (but not $\vec{J}\perp\vec{H}$) case as indicated by theory.[84] Effective H-induced one dimensionality of fluctuation superconductivity in high-ρ_n crystal-

line alloys is also suggested by calorimetric measurements.[81]

(4) The steep resistive onset for $\vec{J}\perp\vec{H}$ occurs somewhat below H_{c2} as defined above (and shown in Fig. 3) by the $\vec{H}||\vec{J} = 3$ A/cm^2 transition. Similar behavior occurs in high-ρ_n crystalline TM superconductors.[83] Comparisons of $H_{c2}(T)$ and $h^*(t)$ as determined from $\vec{H}||\vec{J} = 3$ A/cm^2 and $\vec{H}\perp\vec{J} = 3$ A/cm^2 for $Zr_{0.62}Co_{0.38}$ are shown in Figs. 7 and 13, where the differences are seen to be rather small.

(5) Below the steep resistive onset there is a marked J dependence of the R/R_N vs H curves, which reflects flux-pinning and flux-flow characteristics of the mixed state. Figure 4 shows that flux depinning in $Zr_{0.7}Ni_{0.3}$ occurs at extremely low critical supercurrent density J_c, for example, $J_c = 0.3$ A/cm^2 at $H = 12$ kG $(h \equiv H/H_{c2} = 0.52)$ and $T = 2.2$ K $(t \equiv T/T_c = 0.73)$. This implies a bulk critical pinning force per unit volume[85] $f_c = J_c B = 0.36 \times 10^4$ N/m^3. Table IV compares critical volume pinning forces f_c at similar reduced magnetic fields h and temperatures t for various low-pinning superconductors reported in the literature. The presently measured f_c for as quenched $Zr_{0.7}Ni_{0.3}$ appears to be somewhat greater than those measured in granular aluminum films[86–88] at rather low H, comparable to that measured in $Zr_{0.85}Si_{0.15}$,[89] and less than those measured in annealed crystalline alloys[83,90] and other amorphous metals.[82,91,92] Work is in progress[93] to study f_c as a function of annealing[94] and fabrication procedures. One expects low f_c in materials which are homogeneous on a scale of the coherence distance $\xi_G(T)$, as might be expected in some amorphous alloys, especially those displaying "well-behaved" upper critical fields $H_{c2}(T)$.[27] Interest in such "soft"[89] type-II amorphous superconductors with low-f_p and large zero-temperature Ginzburg-Landau penetration depth $(\lambda_{G0} \approx 7000-10000$ Å for the present alloys as estimated by standard formulas[39]) parallels that in soft amorphous ferromagnets.[1,7] Attention to soft superconductors centers on gaining greater insight into vortex pinning,[82] unbinding,[95] and flow,[96] and in their use for quantum devices.[1,97]

(6) Figure 5 shows the well-known[98] "dip effect" in mixed state $R(H)$, occurring here at $J = 3$ A/cm^2. A vestigal dip effect is also apparent in Fig. 4 at $J = 0.3$ A/cm^2, $T = 2.2$ K. The dip effect is a flux-flow reflection of the more commonly discussed[99] (but not well understood) "peak effect" in J_c vs H and in magnetization M vs H.[39]

C. Temperature dependence of upper critical fields $H_{c2}(T)$—qualitative

Figures 7–10 show upper critical curves $H_{c2}(T)$ constructed from resistive data for $\vec{H}||\vec{J} = 3$ A/cm^2

UPPER CRITICAL FIELDS AND SUPERCONDUCTING . . .

TABLE IV. Volume flux-pinning force for various low-pinning superconductor.

Material (1)	Form (2)	Preparation (3)	J_c[a] (A/cm^2) (4)	H[b] (kG) (5)	f_c[c] $(10^4 \ N/m^3)$ (6)	h[d] (7)	t[e] (8)	Ref. (9)
Al	granular	evaporated	$<5\times10^{-3}$	1.0	$<5\times10^{-4}$	~0.01	0.745	87
Al	granular	evaporated	210	0.011	0.23	0.053	0.75	88
$Zr_{0.70}Ni_{0.30}$	amorphous	melt spun	0.3	12	0.36	0.52	0.73	present work
$Zr_{0.85}Si_{0.15}$	amorphous	melt spun	0.8	7	0.56	0.50	0.83	89
$Nb_{0.95}Mo_{0.05}$	bcc	zone passed	6	2.1	1.3	0.50	0.53	90
$Ti_{0.84}Mo_{0.16}$	bcc	annealed	3	9	2.7	0.47	0.83	83
$Nb_{0.75}Sn_{0.25}$	amorphous	sputtered	6.3	12	7.6	0.50	0.70	82
$(Mo_{0.6}Ru_{0.4})_{0.82}B_{0.18}$	amorphous	arc hammered, cold rolled 14%			13	0.5	0.68	91
$(Mo_{0.6}Ru_{0.4})_{0.82}B_{0.18}$	amorphous	arc hammered			19	0.5	0.68	91
$(Mo_{0.6}Ru_{0.4})_{0.8}Si_{0.1}B_{0.1}$	amorphous	piston anvil	50	12.5	62	0.5	0.82	92

[a]Critical current density (onset voltage criteria vary but this probably has only a minor effect on the comparisons).
[b]Magnetic field applied perpendicular to plane of specimen and to current density J, assumed to be the same as B in the specimen.
[c]Critical volume pinning force $f_c = J_c B$ as discussed in the text.
[d]Reduced field, H/H_{c2}.
[e]Reduced temperature, T/T_c.

(such as that of Figs. 3—5) for all specimens. The curves drawn through the data points are approximate best fits as determined visually. The "error bars" on some data points in Figs. 8—10 indicate the

discrepancy in H_{c2} as determined in separate runs with the 30- and 140-kG magnets. In the region of overlap (~ 10—25 kG), discrepancies for other points were less than the diameters of the closed-circle data points. The superconducting transition temperatures T_c (Table III, column 2) are determined by extrapolating the $H_{c2}(T)$ vs T curves to zero H.
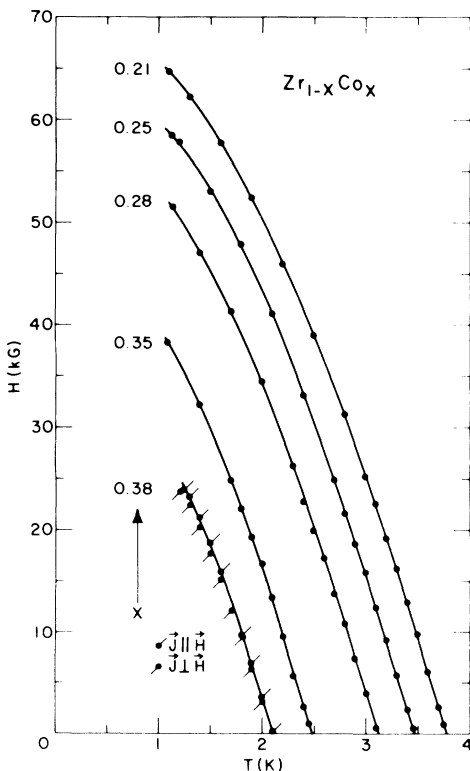
FIG. 7. Upper critical field H_{c2} vs temperature T for amorphous $Zr_{1-x}Co_x$.
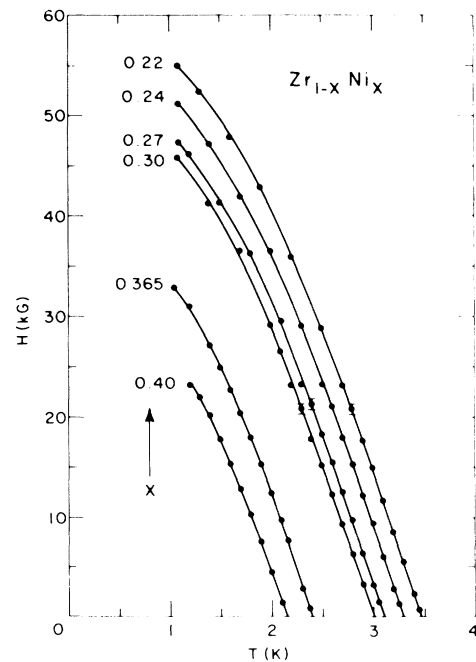
FIG. 8. Upper critical field H_{c2} vs temperature T for amorphous $Zr_{1-x}Ni_x$.
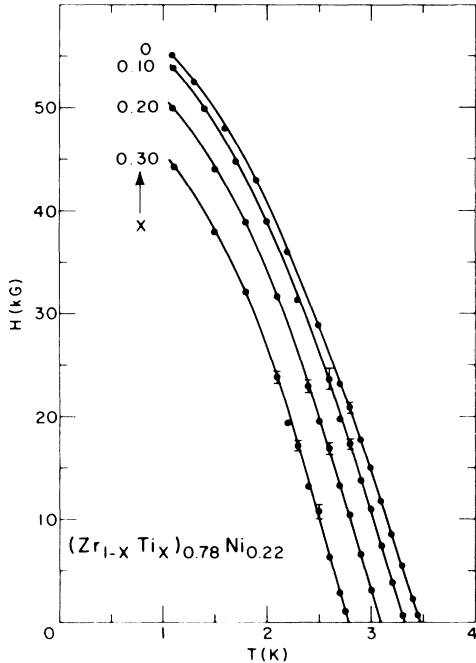
FIG. 9. Upper critical field H_{c2} vs temperature T for amorphous $(Zr_{1-x}Ti_x)_{0.78}Ni_{0.22}$.

The $H_{c2}(T)$ curves of Figs. 7–10 are qualitatively alike: linear in T at low fields near T_c, but with negative curvature in T at higher fields below T_c. In the latter respect they are similar to $H_{c2}(T)$ measured for dirty TM *crystalline* superconductors[37–39] and for amorphous TM superconductors reported by Togano and Tachikawa,[20] Kästner *et al.*,[26] Carter
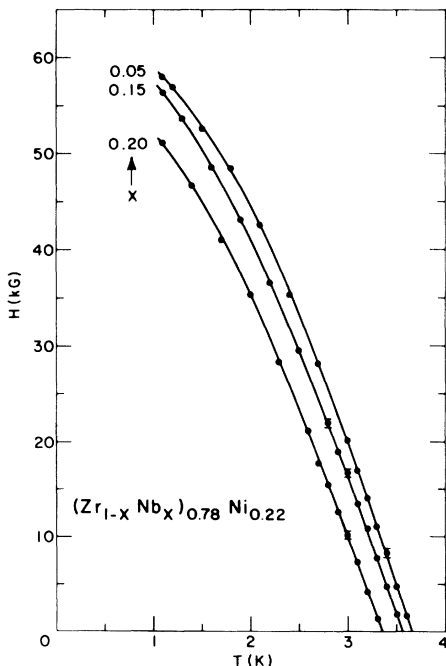
FIG. 10. Upper critical field H_{c2} vs temperature T for amorphous $(Zr_{1-x}Nb_x)_{0.78}Ni_{0.22}$.
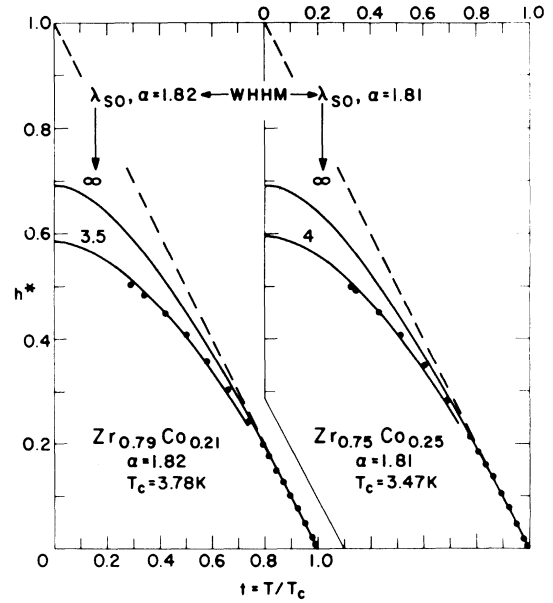
FIG. 11. Reduced upper critical field $h^* \equiv H_{c2}(t)/(-dH_{c2}/dt)_{t=1}$ vs reduced temperature $t \equiv T/T_c$ for amorphous $Zr_{0.79}Co_{0.21}$ and $Zr_{0.75}Co_{0.25}$.

et al.,[27] ourselves[28], and more recently by Samwer and Löhneysen,[29] Eschner and Gey,[30] and Poon *et al.*[31] As previously indicated, the negative curvature at higher H below T_c contrasts sharply with anomalous $H_{c2}(T)$ that is nearly linear in T down to $T/T_c < \sim 0.5$ (TL) observed[23] in metallic glasses (a) based on Mo and stabilized by metalloids,[23,25] and
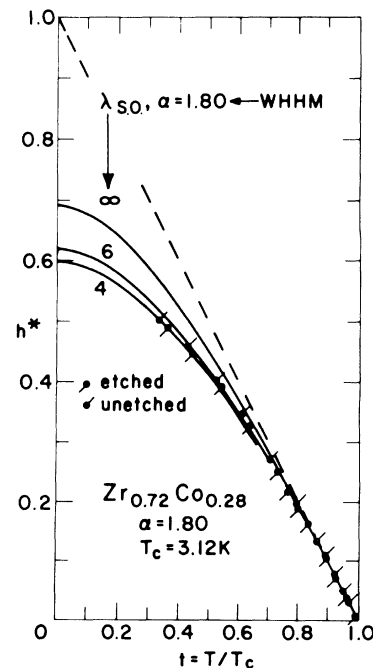
FIG. 12. Reduced upper critical field h^* vs reduced temperature t for amorphous $Zr_{0.72}Co_{0.28}$. The etched and unetched specimens (see text) were cut from the same melt-spun ribbon.
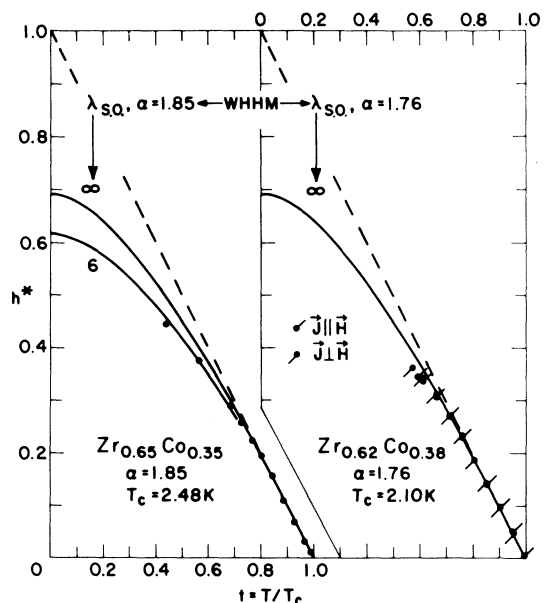
FIG. 13. Reduced upper critical field h^* vs reduced temperature t for amorphous $Zr_{0.65}Co_{0.35}$ and $Zr_{0.62}Co_{0.38}$.

FIG. 15. Reduced upper critical field h^* vs reduced temperature t for amorphous $Zr_{0.73}Ni_{0.27}$ and $Zr_{0.70}Ni_{0.30}$.

(b) of the present Zr-T_L type.[24]

The limiting slopes $(dH_{c2}/dT)_{T_c}$ (Table III, column 3) are not much affected by alloy concentration x for the ZrCo (33—35 kG/K) and ZrNi (30—33 kG/K) series. The slopes are in fair agreement with those reported[24] for two specimens which displayed anomalous TL: $Zr_{0.70}Co_{0.30}$, 33 kG/K; $Zr_{0.70}Ni_{0.30}$, 31 kG/K. For the two pseudo-binary systems $(Zr_{1-x}Ti_x)_{0.78}Ni_{0.22}$ and $(Zr_{1-x}Nb_x)_{0.78}Ni_{0.22}$, $(dH_{c2}/dT)_{T_c}$ increases with in-creasing Ti concentration but decreases with increasing Nb concentration.

D. Comparison of $H_{c2}(T)$ with theory

Figures 11—17 compare upper critical fields[100] for some of the specimens with the predictions of the WHHM theory.[21,22] The conditions for applicability of the WHHM theory are as follows: (a) the dirty limit $\xi_0/l \gg 1$ (Table III, column 16), where

FIG. 14. Reduced upper critical field h^* vs reduced temperature t for amorphous $Zr_{0.78}Ni_{0.22}$ and $Zr_{0.76}Ni_{0.24}$.
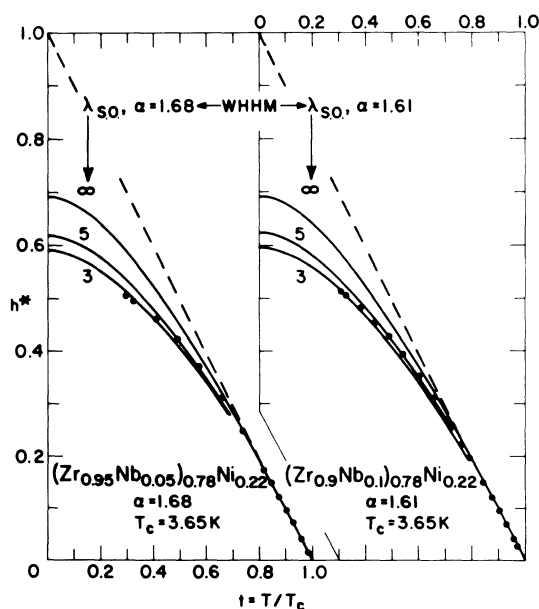
FIG. 16. Reduced upper critical field h^* vs reduced temperature t for amorphous $(Zr_{0.95}Nb_{0.05})_{0.78}Ni_{0.22}$ and $(Zr_{0.9}Nb_{0.1})_{0.78}Ni_{0.22}$.
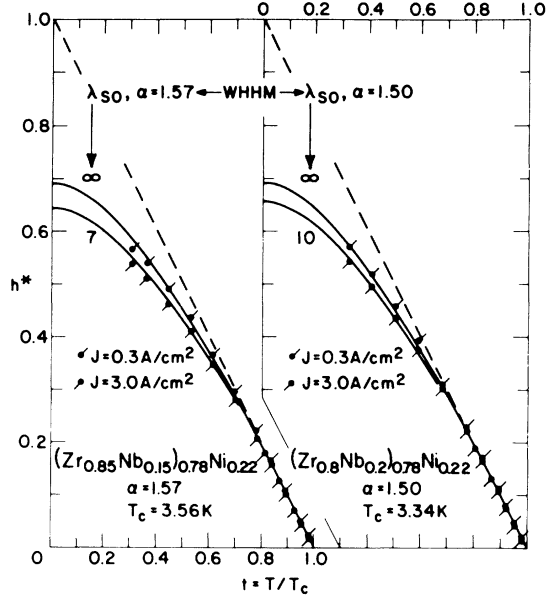
FIG. 17. Reduced upper critical field h^* vs reduced temperature t for amorphous $(Zr_{0.85}Nb_{0.15})_{0.78}Ni_{0.22}$ and $(Zr_{0.8}Nb_{0.2})_{0.78}Ni_{0.22}$. For these two specimens the upper-critical-field resistive transitions are dependent on the current density J (see also Fig. 18).

$\xi_0 = 0.18\hbar v_f (k_B T_c)^{-1}$ is the BCS coherence distance and l (Table III, column 15) is the electron mean free path, (b) large ratio τ_{so}/τ_{tr} (Table III, column 14) of spin-orbit-coupling induced electron-spin-flip scattering time τ_{so} (Table III, column 12) to transport scattering time τ_{tr} (Table III, column 13), (c) BCS weak[101] coupling (half-energy gap $\sim 1.76k_B T_c$, electron-phonon interaction parameter[102] $\lambda_{e\text{-ph}} < \sim 1$), see Sec. IV, (d) specimen spatial homogeneity[27] down to a scale ξ_{G0} (Table III, column 10), (e) electronic structure isotropy (as expected in high-ρ_n crystalline and amorphous alloys), (f) effective three dimensionality (effective specimen dimensions $d \gg \xi_{G0}$).

Figures 11–17 show $H_{c2}(T)$ vs T data plotted in terms of reduced field $h^*(t) \equiv H_{c2}(T)/ -[dH_{c2}(t)/dt]_{t=1}$ versus reduced temperature $t \equiv T/T_c$. The Maki[22] paramagnetic limitation parameter α (Table III, column 4) is experimentally determined from the measured slope $(-dH_{c2}/dT)_{T_c}$, and the spin-orbit scattering parameter[21,103] $\lambda_{so} \equiv 2\hbar (3\pi k_B T_c \tau_{so})^{-1}$ (Table III, column 11) is treated as a fitting parameter.

A notable feature of Figs. 11–16 (and of similar figures[42] not shown here for the other specimens) is the fair agreement with WHHM theory:

(1) Experimental $h^*(t)$ data points lie reasonably close to the theoretical $h^*(\alpha, \lambda_{so}, t)$ curves for $2 \leq \lambda_{so} \leq 6$ values (Table III, column 11) which are

physically reasonable, i.e., they imply spin-orbit-coupling induced spin-flip scattering times τ_{so} much longer than the ordinary transport scattering times τ_{tr} (a condition also required for applicability of the WHHM[21,22] theory). By excluding the last two alloys of Table III, estimated τ_{so}/τ_{tr} ratios (Table III, column 14) are in the range 100–600.

(2) As reduced temperature t decreases, the $h^*(t)$ data points fall near theoretical $h^*(t)$ curves characterized by lower λ_{so} than the theoretical curves which describe the higher-t data. This same type of discrepancy between experiment and WHHM theory has been previously noted[39] for high-ρ_n crystalline TM alloys.

More striking deviations between experiment and WHHM theory have been reported by Orlando et al.[104] for Nb_3Sn specimens where a nonphysical $\tau_{so}/\tau_{tr} < 1$ is required to fit the data. These workers have suggested that neglect of proper many-body renormalization may cause the theory to yield unrealistically low values of τ_{so} (i.e., unrealistically high values of λ_{so} when λ_{so} is regarded as a fitting parameter to experimental data).

Aside from the present and our past[28] measurements, the only relatively low-λ_{so} fits of amorphous alloy $H_{c2}(T)$ data to WHHM theory appear to be those for $Zr_{0.77}Rh_{0.23}$ $(\lambda_{so}=8)$,[20] various ZrRh and ZrPd alloys $(1.8 \leq \lambda_{so} \leq 3.7)$,[30] $Zr_{0.75}Ni_{0.25}$ $(\lambda_{so}=2)$,[31] and $Zr_{0.75}Rh_{0.25}$ $(\lambda_{so}=2)$.[31] High-λ_{so} fits to WHHM have been reported for vapor quenched $Mo_{0.6}Ru_{0.4}$ $(\lambda_{so}=\infty)$,[27] $Mo_{0.52}Ge_{0.48}$ $(\lambda_{so}=\infty)$,[27] sputtered $Mo_{0.45}Si_{0.25}$ $[H_{c2}(T=0)$ exceeds the $\lambda_{so}=\infty$ prediction by 15%],[105] and sputtered $La_{0.78}Zn_{0.22}$ $(\lambda_{so}=\infty$ but apparently in the non-WHHM strong coupling regime).[106] It is possible that strong coupling corrections,[107] extensions of WHHM to the low-τ_{so}/τ_{tr} regime,[108] or renormalization[104] would yield lower λ_{so} values such that $\tau_{so}/\tau_{tr} > 1$ for the above high-λ_{so} cases.

Another possibility is that high-λ_{so} fits to WHHM may reflect some degree of alloy inhomogeneity. Figure 17 shows relatively high-λ_{so} fits for $(Zr_{1-x}Nb_x)_{0.78}Nb_{0.22}$ with $x=0.15,0.20$. Although there is no apparent evidence of alloy inhomogeneity in these specimens in x-ray, density, or normal-state electrical resistivity measurements, other superconductive evidence suggests inhomogeneity:

(1) Figure 18 shows that for $x=0.2$ the resistive transitions for $\vec{H}||\vec{J}$ depend upon the current density J (similar but less pronounced dependence occurs for $x=0.15$). If H_{c2} is defined by the $\vec{H}||\vec{J}=0.3$ A/cm^2 curves, then Fig. 17 shows that $H_{c2}(T)$ lies close to the WHHM theory curve for $\lambda_{so}=\infty$.

(2) Figures 6 and 18 show that the upper-critical-field transition breadths $\Delta H(T)$ are unusually large for these specimens. Extrapolation of $\Delta H(T)$ to T_c
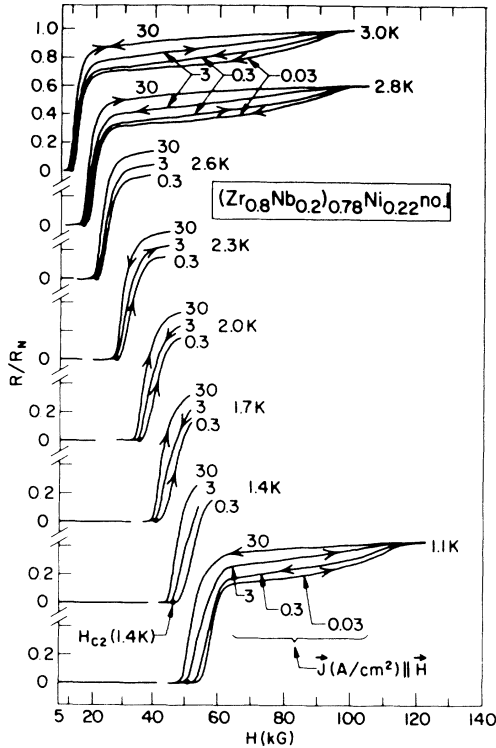
FIG. 18. Resistive transitions for amorphous $(Zr_{0.8}Nb_{0.2})_{0.78}Ni_{0.22}$ as discussed in the text. The J-dependent transition curves above H_{c2} shown at $T=3.0$, 2.8, and 1.1 K demonstrate the beak effect. Note also the J dependence of the resistive transitions near H_{c2}.

and application of Eq. (1) then yields relatively large zero-H breadths $\Delta T(T_c)=74$ and 140 mK (Table I, column 9) for these specimens.

(3) Figure 18 shows a high-H, J-dependent "beak effect" (not to be confused with the peak effect[99] discussed above in connection with Fig. 5) measured at $T=3.0$, 2.8, and 1.1 K. The beak effect was absent in the $(Zr_{0.85}Nb_{0.15})_{0.78}Ni_{0.22}$ specimen but has been observed in a poorly melt-spun $Zr_{0.79}Co_{0.21}$ specimen. The beak effect could be caused by high-T_c crystalline or amorphous inclusions.

IV. ELECTRONIC SPECIFIC-HEAT COEFFICIENTS

The electronic specific-heat coefficients γ_v (per unit volume) (Table III, column 6) are calculated from the limiting upper-critical-field slope in accordance with the Bardeen-Cooper-Schrieffer—Ginzburg-Landau-Abrikosov-Gor'kov relationship[109]

$$\gamma_v = \frac{k_B \pi^3}{12ec} \frac{1}{\rho_n} \left| \frac{-dH_{c2}}{dT} \right|_{T_c}, \qquad (2)$$

where in useful units[39] $k_B\pi^3(12ec)^{-1}=2.268\times10^4$

erg $(\mu\Omega\,cm)\,cm^{-3}\,K^{-1}\,kG^{-1}$, Eq. (2) is applicable in the weak coupling dirty-limit regime. A recent survey[18] comparing γ_v values as calculated from Eq. (2) with calorimetric determinations shows generally good agreement of the two methods, as was also discussed in Ref. 28. The applicability of Eq. (2) is of special physical significance for TM, since it suggests that the same [presumably hybridized (sp)-d] electrons which contribute to the zero-H superconducting transition specific-heat jump $\Delta C \approx 1.4\gamma T_c$ also determine the normal-state resistivity ρ_n.

The electronic specific-heat coefficients γ_m (per mole) (Table III, column 7) are obtained from γ_v and the density-determined atomic volumes V_0 (Table I, column 11). The "dressed," one-spin-state densities of the Fermi level N_γ (Table III, column 8) are then given by

$$N_\gamma = (1 + \lambda_{e\text{-ph}} + \lambda_{es})N_b = (\tfrac{2}{3}\pi^2 k_B^2)^{-1}\gamma_m, \qquad (3)$$

where, in useful units,[39] $(\tfrac{2}{3}\pi^2 k_B^2)^{-1}=0.212$ single-spin states $eV^{-1}atom^{-1}mJ^{-1}$ $(mol\,K^2)$, the λ's are many-body interaction parameters (not to be confused with λ_{so}) with subscripts e-ph, the electron-phonon, and es, the electron-spin fluctuations,[104] and N_b is the "bare" or "band" density of states at the Fermi level.

Figures 19 and 20 show the molar specific-heat coefficients γ_m versus concentration x for the $Zr_{1-x}Co_x$ and $Zr_{1-x}Ni_x$ systems. For both systems γ_m appears to decrease with alloy concentration x although the large $(\pm10\%)$ error bars (reflecting primarily the geometric uncertainty in ρ_n values) preclude any quantitative confidence in the γ_m vs x slope. A rather similar decrease in $\gamma_m(x)$ has recently been reported in other $Zr_{1-x}(T_L)_x$ alloys where $T_L = Cu$,[29] Rh,[30] and Pd.[30]

For the two pseudobinary systems $(Zr_{1-x}Nb_x)_{0.78}Ni_{0.22}$ and $(Zr_{1-x}Ti_x)_{0.78}Ni_{0.22}$, the γ_m values (Table III, column 7) show variation which is small in comparison with the experimental uncertainty, and calorimetric measurements would be useful. Figure 19 shows a rather large (30%) discrepancy of our interpolated γ_m value for $Zr_{0.70}Co_{0.30}$ with that determined from ρ_n and $(dH_{c2}/dT)_{T_c}$ by Tenhover and Johnson.[24] This disagreement arises primarily because the latter measure (with no uncertainty specification) a value $\rho_n = 145\ \mu\Omega\,cm$, much lower than present values for ZrCo (Table III, column 5). Figure 20 shows that present γ_m values for $Zr_{1-x}Ni_x$ are in good agreement with those of Tenhover and Johnson[24] [from ρ_n and $(dH_{c2}/dT)_{T_c}$] and Moody and Ng[110] (from calorimetry), but in marked disagreement (30%) with calorimetric data of Ravex et al.[111] on sput-
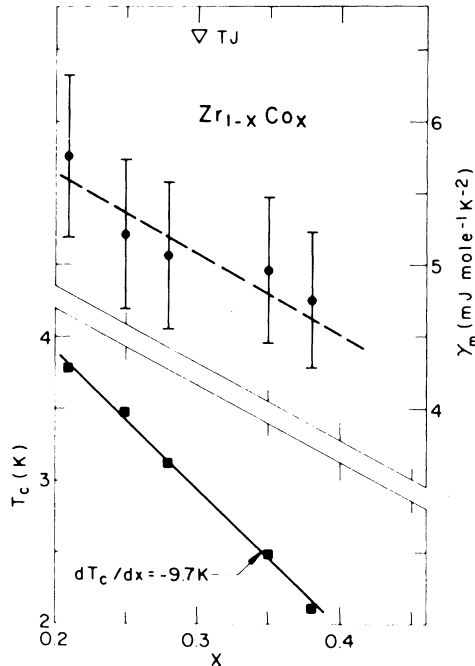
FIG. 19. Superconducting transition temperature T_c and molar specific-heat coefficient γ_m vs alloy concentration x for amorphous $Zr_{1-x}Co_x$. Experimental uncertainty in γ_m of $\pm 10\%$ derives primarily from geometric uncertainty in normal-state resistivity ρ_n used to calculate γ_v from Eq. (2). Other data: Tenhover and Johnson (TJ), Ref. 24.
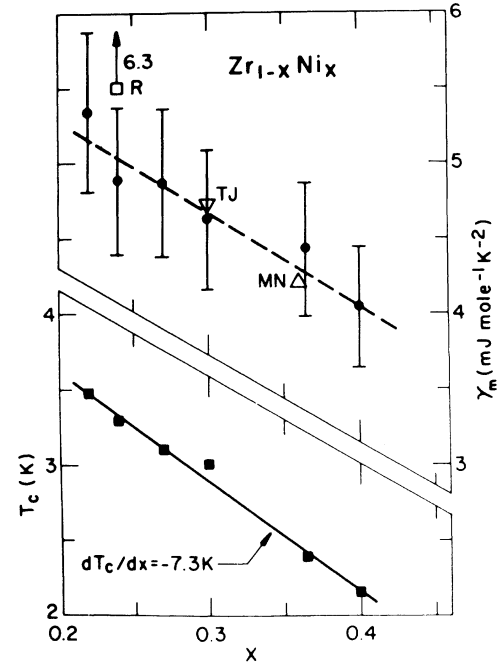
FIG. 20. Superconducting transition temperature T_c and molar specific-heat coefficient γ_m vs alloy concentration x for amorphous $Zr_{1-x}Ni_x$. Experimental uncertainty in γ_m of $\pm 10\%$ derives primarily from geometric uncertainty in normal-state resistivity ρ_n used to calculate γ_v from Eq. (2). Other data: Tenhover and Johnson (TJ), Ref. 24; Moody and Ng (MN), Ref. 110; Ravex et al. (R, sputtered and annealed), Ref. 111.

tered and annealed $Zr_{0.76}Ni_{0.24}$.

Moody and Ng[110] inserted their calorimetrically determined values of $T_c = 2$ K (lower than reported by others, see Fig. 23) and Debye temperature $\Theta_D = 235$ K into the McMillan[102] equation,

$$\lambda_{e\text{-ph}} = \frac{1.04 + \mu^* \ln(\Theta_D/1.45T_c)}{(1-0.62\mu^*)\ln(\Theta_D/1.45T_c) - 1.04},$$

(4)

where μ^* is the Coulomb pseudopotential, which must be guessed [$\mu^* \approx 0.13$ (Ref. 102)], and thereby crudely estimated $\lambda_{e\text{-ph}} \approx 0.5$ for amorphous $Zr_{0.64}Ni_{0.36}$, near the 0.41 estimated[102] for pure hcp Zr. Other similarly derived very approximate $\lambda_{e\text{-ph}}$ values for amorphous Zr-based alloys are $Zr_{1-x}Cu_x$ (0.45–0.64),[29] $Zr_{0.70}Pd_{0.30}$ (0.61),[4] and $Zr_{1-x}Rh_x$ and $Zr_{1-x}Pd_x$ (0.6–0.8).[30] Tunneling data, so as to derive $\lambda_{e\text{-ph}}$ with more certainty from[102] $\alpha^2 F(\omega)$, would be desirable. These relatively low approximate $\lambda_{e\text{-ph}}$ values for Zr-based amorphous alloys help to justify the applicability of Eq. (2) and the weak coupling WHHM theory to the present specimens.

Ultraviolet photoelectron spectroscopy (UPS) data

on various amorphous $Zr\text{-}T_L$ alloys where $T_L = Pd,^{112}$ $Cu,^{112,113}$ $Ni,^{114-116}$ $Co,^{114,116}$ and Fe (Ref. 114) indicate a split-band structure for ZrPd and ZrCu with the Pd and Cu d band lying well below the Fermi level. In these alloys the main contribution to N_b apparently arises from the Zr d band and the (bare) "density of states at the Fermi level is slightly *reduced* compared to pure Zr"[112] (present italics). Furthermore, "replacing Cu by Ni, Co, and Fe, i.e., going to the left in the first series of transition metals, the *separation of the two d-band peaks is decreased.*"[114]

The present γ_m values (Table III, column 7) for amorphous ZrCo (4.8–5.8 in units of mJ mole^{-1} K^{-2} here and below) and ZrNi (4.0–5.3), considered along with those determined calorimetrically[29] for $Zr_{1-x}Cu_x$ (3.4–4.5) are all higher than the $\gamma_m = 2.91$ (Table II, column 10) for pure hcp Zr, suggesting bare-state densities at the Fermi level N_b which are *greater* than the N_b (cZr) = 0.42 single-spin states eV^{-1} atom^{-1} estimated[102] for crystalline Zr. Analysis[29] of calorimetric data on $Zr_{1-x}Cu_x$, assuming $\lambda_{es} = 0$, using Eq. (4) to estimate $\lambda_{e\text{-ph}} = 0.45$–0.64, and employing Eq. (3) to find N_b yields (here and below in the same units as above)

N_b $(Zr_{1-x}Cu_x)=0.48-0.56$, somewhat above $N_b(cZr)$ and contrary to the UPS interpretation.[112] If we assume that for all amorphous $Zr_{1-x}Co_x$ and $Zr_{1-x}Ni_x$ alloys, $\lambda_{e\text{-ph}}\approx0.6$ [near those estimated for $Zr_{0.64}Ni_{0.36}$,[110] $Zr_{1-x}Cu_x$,[29] and $Zr_{0.7}Pd_{0.3}$ (Ref. 4)] and use Eq. (3) with $\lambda_{es}=0$ to obtain N_b, then N_b $(Zr_{1-x}Co_x)=0.64-0.77$ and N_b $(Zr_{1-x}Ni_x)$ $=0.53-0.62$. The UPS indicated[114] band-merging effect as one replaces Cu by Ni and Co could account for the apparent increase in N_b for ZrCo and ZrNi over that in ZrCu, as previously suggested by Tenhover and Johnson,[24] but calorimetric and tunneling data would be useful in assessing this possibility.

In any event, the presently observed TM-like high γ_m values, as well as those reported for other $Zr_{1-x}(T_L)_x$ alloys where $T_L=Cu$,[29] Rh,[30] and Pd (Refs. 4 and 30) are not easily explained on the basis of nearly-free-electron models sometimes applied in liquid and amorphous alloy treatments of electron-transport[117] and structural stability.[118] The γ_v values calculated from Eq. (2), along with measured ρ_n values have been used to calculate the Ginzburg-Landau (GL) extrinsic $\kappa_I=76-92$ (Table III, column 9), and the GL zero-temperature coherence distance $\xi_{G0}=50-70$ Å (Table III, column 10). In order to estimate the transport scattering time τ_{tr} we have arbitrarily and rather nonphysically assumed (as previously[39] in treating high-ρ_n crystalline TM alloys) an effective conduction-electron density $n=\langle e/a\rangle V_0^{-1}$ and that S/S_f (the ratio of free Fermi surface area S to that of a free-electron gas of density n) is 0.6. The values for τ_{tr}, τ_{so}/τ_{tr}, the electron mean free path l, and the dirtiness parameter ξ_0/l in Table III, columns 13—16 then follow from standard formulas[39] as indicated in the Table III footnotes. If we assume, on the other hand, a free-electron-like Fermi surface $S/S_f=1$, and $n=\langle e/a\rangle V_0^{-1}$, but with $e/a=3,2,2,0$ for Nb, Zr, Ti, and T_L $(T_L=Ni,Co)$, respectively, then the combined n decrease and S/S_f increase multiply the τ_{tr} values (Table III, column 13) by factors of 1.7—3.4, the τ_{so}/τ_{tr} values (Table III, column 14) by 0.6—0.3, the l values (Table III, column 15) by 1.3—1.8, and the ξ_0/l values (Table III, column 16) by 0.6—0.3. Thus the order of magnitude of τ_{tr} and τ_{tr}-dependent parameters (Table III, columns 13—16) does not appear to depend critically on assumptions regarding the effective conduction-electron density or Fermi-surface ratios.

The very high $\xi_0/l=300-1300$ values (Table III, column 16) indicate that the present amorphous alloys are among the dirtiest superconductors ever examined and perhaps approach Pippard's[119] hundred percent dirty superconductor: "As you go on adding impurity, and physical strain, and defects, and this,

that, and the other sort of filth to superconductors ... is there any limit to which you can reasonably expect to attain? That is to say, is there such a thing as a hundred percent dirty superconductor, and if we do make a hundred percent dirty superconductor will it have properties as ideal as one that is a hundred percent pure?" Some near-ideal properties of the present specimens are summarized in Sec. VI below.

V. SUPERCONDUCTING TRANSITION TEMPERATURES

Figures 19—21 show the superconducting transition temperature T_c (Table III, column 2) versus alloy concentration for the four amorphous alloy series. Figures 19 and 20 show that for $Zr_{1-x}Co_x$ and $Zr_{1-x}Ni_x$ alloys, T_c decreases linearly with x with slopes $dT_c/dx=-9.7$ and -7.3 K/atomic fraction, respectively. These slopes may be compared with those reported for ZrCo (-12) (Ref. 56) and ZrNi (-6.3) (Ref. 67) (in the same units). As indicated above, for these series the molar electronic specific-heat coefficient γ_m also appears to decrease in rough parallel with T_c as shown in the same fig-
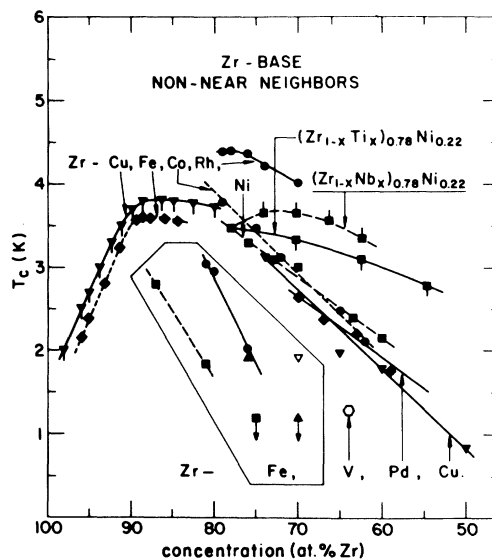
FIG. 21. Superconducting transition temperature T_c vs concentration for Zr in amorphous $(Zr_{1-x}Ti_x)_{0.78}Ni_{0.22}$ and amorphous $(Zr_{1-x}Nb_x)_{0.78}Ni_{0.22}$ (top right). For comparison the T_c variation of other amorphous Zr-based alloys is also shown: ZrCu (▼) and ZrFe (♦), Ref. 120; ZrFe (■), Ref. 6; ●, Ref. 56; ▲, Ref. 28; ∇, Refs. 24 and 121; V (○), Ref. 24; Co (●) and Ni (■) present work; Cu (▼), Ref. 29; Pd (♦), Ref. 122; Rh (●), Ref. 30. The vertical arrows on the two lowest ZrFe points mean that the T_c's are below 1.2 K.
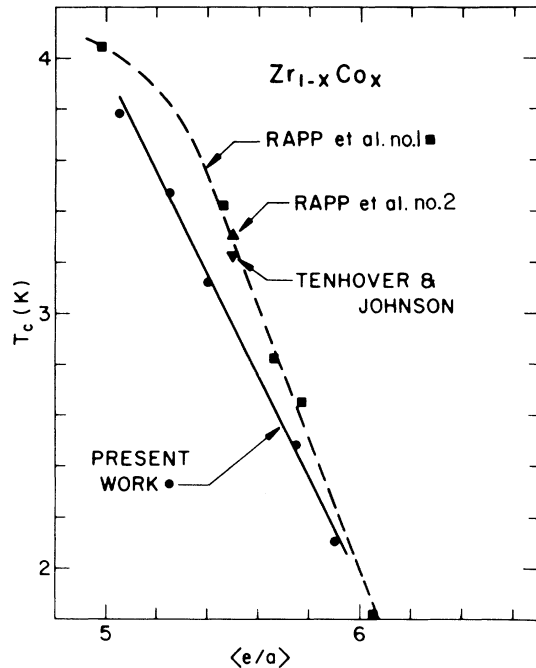
FIG. 22. Superconducting transition temperature T_c vs average electron-to-atom ratio $\langle e/a \rangle$ for amorphous $Zr_{1-x}Co_x$. Here as elsewhere $\langle e/a \rangle$ is the conventional Matthias-count average number of electrons outside closed shells of the free atom. Other data: Rapp *et al.* no. 1, Ref. 55; Rapp *et al.* no. 2, Ref. 69; Tenhover and Johnson, Ref. 24.
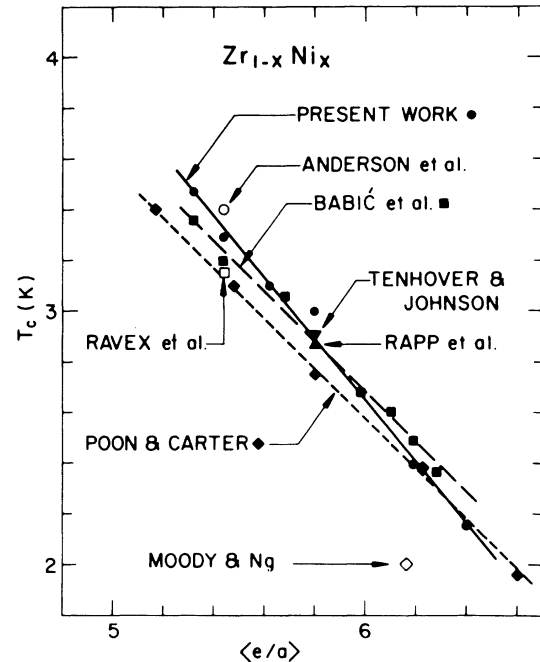
FIG. 23. Superconducting transition temperature T_c vs average electron-to-atom ratio $\langle e/a \rangle$ for amorphous $Zr_{1-x}Ni_x$. Other data: Anderson *et al.*, Ref. 94; Babić *et al.*, Ref. 67; Tenhover and Johnson, Ref. 24; Rapp *et al.*, Ref. 69; Ravex *et al.* (as sputtered), Ref. 111; Poon and Carter, Ref. 123; Moody and Ng, Ref. 110.

ures. Figure 21 shows that in the pseudobinary systems $(Zr_{1-x}Ti_x)_{0.78}Ni_{0.22}$ and $(Zr_{1-x}Nb_x)_{0.78}Ni_{0.22}$, T_c decreases with Ti concentration, whereas T_c first increases and then decreases with Nb concentration. As indicated previously, for both these systems the γ_m variation is considerably less than the experimental uncertainty in γ_m of $\pm 10\%$.

Figures 22 and 23 show T_c versus the average "valence" electron-to-atom ratio $\langle e/a \rangle$ for amorphous ZrNi and ZrCo alloys. Here $\langle e/a \rangle$ is the conventional "Matthias-count"[124] average number of electrons outside closed shells of the free atom. Figure 22 shows that the present T_c values for $Zr_{1-x}Co_x$ are as much as 12% lower than those of other investigators,[24,55,69] possibly due to our use of relatively low purity Co (Table II, column 4). On the other hand, Fig. 23 indicates reasonably good agreement of present T_c values for $Zr_{1-x}Ni_x$ with those reported by most others.[24,67,69,94,110,111,123]

Figure 24 shows T_c vs $\langle e/a \rangle$ for the two pseudobinary systems. For comparison the presently indicated curves for T_c vs $\langle e/a \rangle$ for amorphous ZrCo and ZrNi are also shown. The decrease in T_c with Ti concentration in $(Zr_{1-x}Ti_x)_{0.78}Ni_{0.22}$ is opposite to the behavior of crystalline hcp $Zr_{1-x}Ti_x$ alloys,

where T_c (and also γ_m) increase[125] with x for $0 \leq x \leq 0.5$. The peaking of T_c with increase of $\langle e/a \rangle$, shown by $(Zr_{1-x}Nb_x)_{0.78}Ni_{0.22}$, has apparently not been previously observed in $T_E T_L$ alloys *quenched from the melt*, except for a very small effect in recent data[30] on low Rh concentration ZrRh alloys (see Figs. 21 and 25). A split-band interpretation of the $T_c(x)$ peak in $(Zr_{1-x}Nb_x)_{0.78}Ni_{0.22}$ might be that the high niobium d band (unlike the Ni d band[114-116]) falls close to the Fermi level, thus elevating N_b and thus T_c. Calorimetric and UPS data would, of course, be helpful in elucidating the present pseudobinary alloy behavior.

Figure 25 shows curves of T_c vs $\langle e/a \rangle$ for three classes of TM amorphous alloys:

(1) The top curve shows the well-known Collver-Hammond peak[9] for $4d$ vapor-quenched amorphous alloys between nearest and next-nearest neighbors in the Periodic Table. This curve peaks at $\langle e/a \rangle = 6.4$, $T_c = 9.4$. (A similar curve obtains for $5d$ near-neighbor vapor-quenched alloys.[9,10])

(2) Within the delineated border situated under the Collver-Hammond peak are curves and data points for amorphous ZrT_L alloys, all quenched from the melt except for the ion-implanted low-
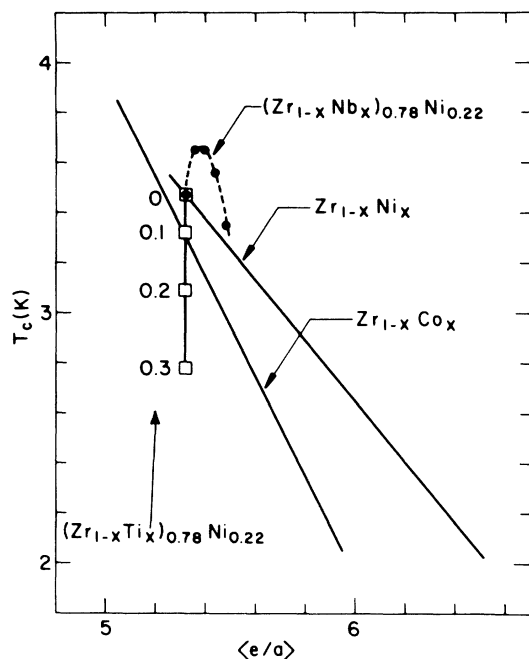
FIG. 24. Superconducing transition temperature T_c vs average electron-to-atom ratio $\langle e/a \rangle$ for amorphous pseudobinary alloys $(Zr_{1-x}Ti_x)_{0.78}Ni_{0.22}$ and $(Zr_{1-x}Nb_x)_{0.78}Ni_{0.22}$. For comparison, curves of T_c vs $\langle e/a \rangle$ for ZrCo and ZrNi as indicated by the present data (Figs. 22 and 23) are also shown.

$\langle e/a \rangle$ ZrCu and ZrFe alloys measured by Meyer et al.[120] and judged[120] to be amorphous partially on the basis of normal-state resistivity data at 4—300 K. The wide scatter in melt-quenched ZrFe data from different laboratories[6,24,28,56,121] is evidently associated with difficulties[42,56,114] in fabricating these specimens and/or sensitivity of the magnetic condition[24,43,56,127] of Fe to details of the processing. Ignoring the melt-quenched ZrFe curves, the T_c vs $\langle e/a \rangle$ data for ZrT_L alloys peak roughly at $\langle e/a \rangle = 4.8$, $T_c = 3.8$ K (4.4 K for ZrRh).

(3) At $\langle e/a \rangle \approx 6.8$ are various T_5T_9 (NbRh, NbIr, TaRh, TaIr) and T_5T_{10} (NbNi) alloys with T_c in the range 1.5—5.2. Here the subscripts indicate the group numbers.

The variety of T_c vs $\langle e/a \rangle$ behaviors shown in Figs. 22—25 is consistent with the early suggestion of Collver and Hammond[10] that "there is no universal T_c vs $\langle e/a \rangle$ curve for all amorphous TM alloys, as there is a breakdown from such a correlation for alloys composed of TM elements widely separated in the Periodic Table."[10] The UPS indication[112-116] of split-band behavior in amorphous T_ET_L alloys is also compatible with the idea that the alloying dependence of their superconducting transition temperature cannot be described by T_c vs $\langle e/a \rangle$ rules. Such rules[124] often hold for near-neighbor crystal-
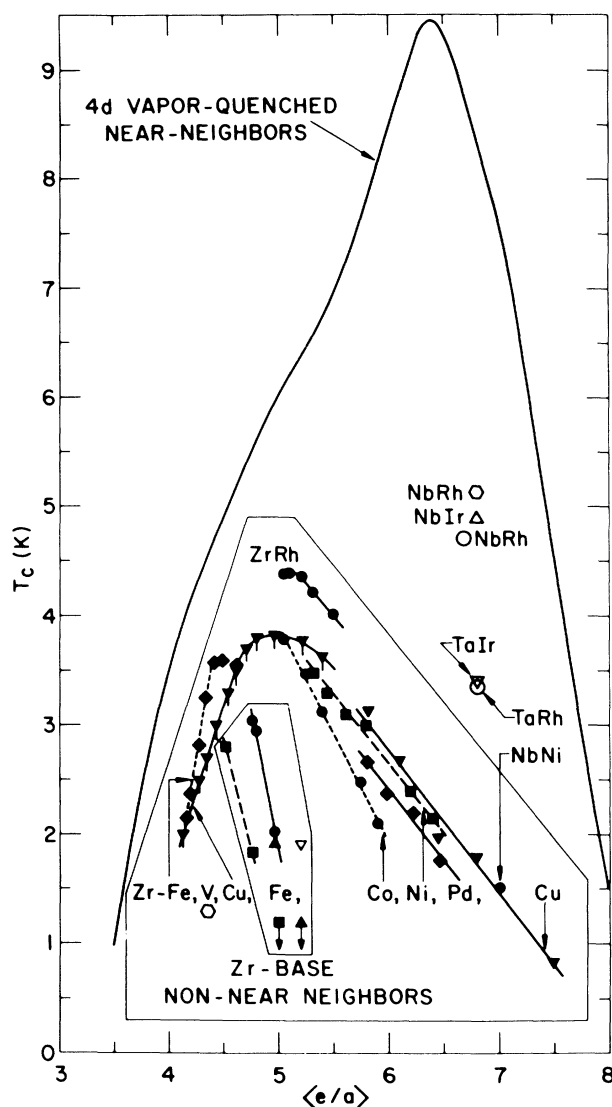
FIG. 25. Superconducting transition temperature T_c vs average electron-to-atom ratio $\langle e/a \rangle$ for $4d$ vapor-quenched "near" (nearest and next-nearest) neighbors (Ref. 9) and various amorphous TM alloys. The data for Zr-based non-near neighbors are due to the following: ZrCu (▼) and ZrFe (◆), Ref. 120; ZrFe (■), Ref. 6; ●, Ref. 56; ▲, Ref. 28; ▽, Refs. 24 and 121; V (O), Ref. 24; Co (●) and Ni (■) present work; Cu (▼), Ref. 29; Pd (◆), Ref. 122; Rh (●), Ref. 30. The vertical arrows on the two lowest ZrFe points mean that the T_c's are below 1.2 K. The data for Nb-based alloys are due to the following: NbRh (O), Ref. 18; o, Ref. 126; NbIr (△), Ref. 18; NbNi (●), Ref. 126. The data for Ta-based alloys are due to Ref. 18. In this plot e/a for Cu has arbitrarily been taken as 11 rather than 1.

line alloys and probably reflect the alloying dependence of the bare-state density N_b as the Fermi level moves along a *collective d* band.[128-131] Rapp et al.[55,56] have also emphasized the limited applica-

bility of T_c vs $\langle e/a \rangle$ rules[132] for TM amorphous alloys.

Figure 21 shows T_c vs Zr concentration for the same amorphous ZrT_L alloy data plotted in Fig. 25. In addition, as previously discussed, Fig. 21 shows the T_c variation of the present pseudobinary alloys. Disregarding the latter (as nonrepresentative of Zr-base alloys), as well as the scattered *melt-quenched* ZrFe data, a somewhat more universal single-peak curve is obtained for Zr-base non-near neighbor alloys than in the corresponding T_c vs $\langle e/a \rangle$ plot of Fig. 25. This implies that equal atomic concentrations of T_L-atom additions have much the same effect on the T_c of amorphous Zr regardless of their group number (at high concentrations Fe may be an exception due to magnetic effects[24,43,56,127]).

It is interesting that Rh (a $4d$ metal) is "out of line" in Figs. 21 and 25 suggesting a possible influence of $3d$-atom (and Pd) spin-fluctuation effects on T_c, although susceptibility measurements on amorphous ZrCo (Refs. 56 and 68) and ZrNi (Refs. 67 and 68) in the present concentration range show no evidence for moment localization or very high Pauli paramagnetism. Likewise, hcp Zr-based alloys with dilute additions of $3d$ elements show magnetic moment localization only for Mn.[133]

T_c variations such as those of Figs. 21 and 25 are usually discussed in terms of the McMillan equation (4) and his expression for the (single-element) electron-phonon coupling parameter[102]

$$\lambda_{e\text{-ph}} = \frac{N_b \langle I^2 \rangle}{m \langle \omega^2 \rangle} , \qquad (5)$$

where $\langle I^2 \rangle$ is the mean-square electron-phonon matrix element, m is the atomic mass, and $\langle \omega^2 \rangle$ is a mean-square phonon frequency.[102] Associated with the fact that little is known about the electronic or vibrational properties of the vapor-quenched $4d$ near-neighbor alloys of Collver and Hammond,[9,10] a variety of different explanations of the Collver-Hammond peak (CHP), all based essentially on Eq. (5), have been offered. Dynes and Varma[134] suggest that CHP is due to the "variation of N_b with changing electron concentration in a smooth structureless fashion with alloying"; Butler[131] regards CHP as reflecting primarily a triangular variation of $\langle I^2 \rangle/(m\langle\omega^2\rangle)$ where the $\langle I^2 \rangle$ contribution is dominant, consistent with his rigid-muffin-tin calculations for $4d$ elements in the cubic crystalline phase; and Bennemann[135] interprets CHP as due primarily to variation in $\langle I^2 \rangle$. As previously pointed out by Chaudhari and Turnbull,[1] Bennemann's analysis appears to be partially based on the questionable assumption that the atomic volume increase on melting of a crystalline material is always close to the in-

crease in atomic volume in going from the crystalline to the amorphous solid. On the other hand, data such as the present density measurements would indicate that in $T_E T_L$ alloys the amorphous and crystalline phases are about equally close packed with packing fractions $\eta \approx 0.74$.

Interpretations of T_c variation in liquid-quenched Zr-based alloys are able to rely on a greater range of experimental information but no satisfactory general description has been achieved. Samwer and Löhneysen's analysis[29] of their calorimetric data[29] on amorphous ZrCu [relying on approximate $\lambda_{e\text{-ph}}$ values deduced from Eq. (4)] indicates that the measured 73% drop in T_c with a Cu addition occurs with a 25% decrease in N_γ, but only a 15% decrease in N_b. They attribute the T_c drop primarily to decrease in $\langle I^2 \rangle$ resulting from dilution of Zr-Zr interaction by the addition of T_L atoms, i.e., the average Zr-Zr atom separation increases as T_L atoms are added. On the other hand, Tenhover and Johnson[24] suggest that their measured 20% decrease in T_c in going from Co to Ni to Cu in the amorphous alloys $Zr_{0.70}Co_{0.30}$, $Zr_{0.70}Ni_{0.30}$, and $Zr_{0.70}Cu_{0.30}$ is associated primarily with a concomitant 36% decrease in N_γ as inferred from their ρ_n and $(dH_{c2}/dT)_{T_c}$ measurements [which (for T_c and ρ_n of $Zr_{0.7}Co_{0.3}$) differ somewhat from the present measurements]. Eschner and Gey[30] conclude [on the basis of calorimetric ρ_n and $(dH_{c2}/dT)_{T_c}$ measurements on amorphous ZrRh, ZrPd, and ZrRhPd alloys] that N_b "has no importance concerning T_c" and that the McMillan equation (4) is "not applicable to amorphous metals." Clearly, more work appears to be required in this area.

On the basis of the somewhat similar $\gamma(x)$ behavior of $Zr_{1-x}Co_x$ (Fig. 19), $Zr_{1-x}Ni_x$ (Fig. 20), and $Zr_{1-x}Cu_x$,[29] one might speculate that the rough congruence of T_c versus composition data for various Zr-$3d$ alloys on the broad single-peak curve of Fig. 21 indicates that the Löhneysen-Samwer dilution-effect[29] lowering of $\langle I^2 \rangle$ plays the key role in depressing T_c in the 50—80 at. % Zr range in all cases. The controlling parameter, average Zr-Zr atom separation, would then correspond to the suggested[131] influential $4d$-atom separation in the near-neighbor CHP case. There, according to Butler,[131] $\langle I^2 \rangle$ peaks near Mo, associated in part with a minimum in atomic separation to the right of Mo in the Periodic Table.[136] One expects a similar minimum for amorphous alloys on the basis of tabulated Goldschmidt radii.[45]

VI. CONCLUSIONS

The present upper-critical-field data on various amorphous, Zr-based TM alloys are in fair agree-

ment with the standard dirty-limit WHHM theory.[21,22] We do not observe gross departure from WHHM in the form of $H_{c2}(T)$ curves that are nearly linear in T down to $T/T_c < {\sim}0.5$ as reported by some,[23–25] nor (with the exception of two specimens) less pronounced deviation from WHHM in the form of $H_{c2}(T)$ curves requiring unphysically high-λ_{so} fits to WHHM as observed by others.[27,105,106] Structure integrity of our specimens is indicated by x-ray, density, bend-ductility, normal-state electrical resistivity, superconducting transition width, and mixed-state flux-pinning measurements. $H_{c2}(T)$ curves that are linear in T down to $T/T_c < {\sim}0.5$ or that indicate high λ_{so} when compared to WHHM may reflect inhomogeneity.[27] Such an interpretation is consistent with present results on two $(Zr_{1-x}Nb_x)_{0.78}Ni_{0.22}$ specimens for which relatively high λ_{so} values derived from WHHM fits are coupled with relatively broad zero-field superconducting transitions, current-density-dependent resistive upper-critical-field transitions, and (in one specimen) a J-dependent, high $H > H_{c2}$ resistive beak effect (Fig. 18).

Estimates of the dirtiness parameter $\xi_0/l \approx 300-1300$ [based on approximate formulas[39] and measured values of T_c, ρ_n, and $(dH_{c2}/dT)_{T_c}$] indicate an approach to Pippard's[119] "100% dirty superconductor." Very dirty superconductors tend to display clean properties.[39] The present alloys [ignoring the two apparently inhomogeneous $(Zr_{1-x}Nb_x)_{0.78}Ni_{0.22}$ specimens] display near ideality in several respects: (a) $H_{c2}(T)$ curves in fair accordance with $dirty$-$limit$ WHHM theory,[21,22] (b) relatively sharp resistive transitions at T_c over $\Delta T(T_c)=4-50$ mK, (c) sharper H_{c2} transitions for current density $\vec{J} \perp \vec{H}$ than for $\vec{J} \| \vec{H}$, consistent with a one-dimensional fluctuation spectrum for $\vec{J} \| \vec{H}$,[84] (d) current-density J independence of H_{c2} transitions for $0.03 \leq J \leq 3$ A/cm^2, (e) critical flux-depinning forces $f_c = J_c H$, lower than reported for most other low-pinning crystalline[83,90] and amorphous[82,91,92] superconductors.

T_c measurements in the amorphous $Zr_{1-x}Co_x$ and $Zr_{1-x}Ni_x$ systems show that T_c decreases linearly with Co or Ni addition in fair agreement with previous results[24,55,67,69,94,110,111,123] on these systems. Upper-critical-field and normal-state electrical resistivity measurements suggest concomitant decrease in the molar electronic specific-heat coefficients. In the $(Zr_{1-x}Ti_x)_{0.78}Ni_{0.22}$ and $(Zr_{1-x}Nb_x)_{0.78}Ni_{0.22}$ systems, T_c decreases with Ti addition, while T_c first increases and then decreases with Nb addition. The wide variety of T_c vs $\langle e/a \rangle$ behavior in the present and in other amorphous alloys (Figs. 22–25) is consistent with the idea[10] (bolstered by recent UPS data[112–116] indicating split bands in amorphous TM alloys) that the alloying dependence of T_c in amorphous superconductors cannot be described by any general T_c vs $\langle e/a \rangle$ rules such as often apply to near-neighbor crystalline alloys.[124]

Satisfactory understanding of T_c variations in amorphous TM alloys as shown in Figs. 21 and 25 appears to require more data (e.g., calorimetric, upper critical field, UPS, neutron inelastic scattering, and tunneling) on well-characterized specimens from a wide variety of different amorphous systems. As in the present work, structural characterization may be assisted by superconductive measurements (e.g., transition breadth, current-density dependence of resistive transitions, upper-critical-field temperature dependence, and mixed-state flux pinning).

*Present address: Département de Physique de la Matière Condensée, Université de Genève, CH-1211 Geneva 4, Switzerland.

[1] P. Chaudhari and D. Turnbull, Science <u>199</u>, 11 (1972); P. Chaudhari, B. C. Giessen, and D. Turnbull, Sci. Am. <u>242</u> (4), 98 (1980); F. E. Luborsky and L. A. Johnson, J. Phys. (Paris) Colloq. <u>41</u>, C8-821 (1980); J. J. Gilman, ibid. <u>41</u>, C8-811; Science <u>208</u>, 856 (1980); P. Gwynne, Mosaic <u>12</u> (6), 15 (1981).

[2] H. Beck and H.-J. Güntherodt, in Glassy Metals I, edited by H.-J. Güntherodt and H. Beck (Springer, Berlin,

1981), p. 1.

[3] N. F. Mott, J. Phys. (Paris) Colloq. <u>41</u>, C8-1 (1980); Philos. Mag. E <u>44</u>, 265 (1981).

[4] W. L. Johnson, in Glassy Metals I, Ref. 2, p. 191.

[5] C. C. Tsuei, in Superconducting Materials Science, edited by S. Foner and B. Schwartz (Plenum, New York, 1981), p. 735.

[6] S. J. Poon, in Amorphous Metallic Alloys, edited by F. E. Luborsky (Butterworth, Washington, D.C., in press).

[7] For recent reviews, see S. Methfessel, in Liquid and

Amorphous Metals, edited by E. Lüscher and H. Coufal (Sijthoff and Noordhoff, Netherlands, 1980), p. 501; G. A. Petrakovskii, Usp. Fiz. Nauk 134, 305 (1981) [Sov. Phys.—Usp. 24, 511 (1981)].

[8]J. H. Mooij, Phys. Status Solidi A 17, 521 (1973).

[9]M. M. Collver and R. H. Hammond, Phys. Rev. Lett. 30, 92 (1973).

[10]M. M. Collver and R. H. Hammond, Solid State Commun. 22, 55 (1977).

[11]For a review see, e.g., H. Jones, in *Treatise on Materials Science and Technology: Ultrarapid Quenching of Liquid Alloys,* edited by H. Herman (Academic, New York, 1981), Vol. 20, p. 1.

[12]W. L. Johnson and S. J. Poon, J. Appl. Phys. 46, 1787 (1975).

[13]W. L. Johnson, S. J. Poon, and P. Duwez, Phys. Rev. B 11, 150 (1975).

[14]R. Koepke and G. Bergmann, Solid State Commun. 19, 435 (1976). These measurements are on vapor-quenched Mo films.

[15]W. L. Johnson, S. J. Poon, J. Durand, and P. Duwez, Phys. Rev. B 18, 206 (1978).

[16]E. Domb and W. L. Johnson, J. Low. Temp. Phys. 33, 29 (1978).

[17]K. Reichelt and G. Bergmann, J. Appl. Phys. 46, 2747 (1975). These measurements are on rf-sputtered WN_x and MoN_x films.

[18]C. C. Koch, D. M. Kroeger, J. O. Scarbrough, and B. C. Geissen, Phys. Rev. B 22, 5213 (1980).

[19]B. M. Clemens, W. L. Johnson, and J. Bennett, J. Appl. Phys. 51, 1116 (1980).

[20]K. Togano and K. Tachikawa, Phys. Lett. 54A, 205 (1975); J. Appl. Phys. 46, 3609 (1975).

[21]N. R. Werthamer, E. Helfand, and P. C. Hohenberg, Phys. Rev. 147, 295 (1966).

[22]K. Maki, Phys. Rev. 148, 362 (1966).

[23]M. Tenhover, W. L. Johnson, and C. C. Tsuei, Solid State Commun. 38, 53 (1981).

[24]M. Tenhover and W. L. Johnson, Physica 108B, 1221 (1981).

[25]C.-H. Strudthoff, J. Reichelt, and H. C. Freyhardt, Physica 107B, 393 (1981).

[26]J. Kästner, H. v. Löhneysen, M. Platte, and K. Samwer, in *Proceedings of the Conference on Metallic Glasses: Science and Technology, Budapest, 1980,* edited by C. Hargitai, I. Bakonyi, and T. Kemeny (Central Research Institute, Budapest, 1980), p. 419.

[27]W. L. Carter, S. J. Poon, G. W. Hull, Jr., and T. H. Geballe, Solid State Commun. 39, 41 (1981).

[28]M. G. Karkut and R. R. Hake, Physica 109&110B, 2033 (1982).

[29]K. Samwer and H. v. Löhneysen, Phys. Rev. B 26, 107 (1982).

[30]W. Eschner and W. Gey, in *Superconductivity in d- and f-Band Metals—1982,* edited by W. Buckel and W. Klose (Kernforschungszentrum, Karlsruhe, W. Germany, 1982), p. 359. For $Zr_{0.71}Pd_{0.29}$, Eschner and Gey obtain (with no uncertainty specification) $\rho_n = 226$

$\mu\Omega$ cm, about 30% *higher* than reported in Ref. 28 for $Zr_{0.70}Pd_{0.30}$. This relatively high ρ_n, when inserted into Eq. (2) [along with $(dH_{c2}/dT)_{T_c} = -30.6$ kG/K, close to that of Ref. 28] yields their quoted $\gamma_m = 3.7$ mJ/moleK^2, about 26% *lower* that measured calorimetrically for $Zr_{0.70}Pd_{0.30}$ by J. E. Grebner, B. Golding, R. J. Schutz, F. S. L. Hu, and H. S. Chen, Phys. Rev. Lett. 39, 1480 (1977).

[31]S. J. Poon, S. K. Hasanain, and K. M. Wong, Phys. Lett. 93A, 495 (1983).

[32]A. F. Ioffe and A. R. Regel, Prog. Semicond. 4, 237 (1960).

[33]R. R. Hake, S. Aryainejad, and M. G. Karkut, in *Superconductivity in d- and f-Band Metals,* edited by H. Suhl and M. B. Maple (Academic, New York, 1980), p. 480.

[34]R. R. Hake, M. G. Karkut, and S. Aryainejad, Physica 107B, 503 (1981).

[35]S. Aryainejad, M. G. Karkut, and R. R. Hake, Bull. Am. Phys. Soc. 27, 222 (1982).

[36]S. Aryainejad, R. R. Hake, and M. G. Karkut (unpublished).

[37]T. G. Berlincourt and R. R. Hake, Phys. Rev. 131, 140 (1963).

[38]Y. B. Kim, C. F. Hempstead, and A. R. Strnad, Phys. Rev. 139, A1163 (1965); L. J. Neuringer and Y. Shapira, *ibid.* 140, A1638 (1965).

[39]R. R. Hake, Phys. Rev. 158, 356 (1967).

[40]B. M. Clemens, M. Tenhover, and W. L. Johnson, Physica 107B, 319 (1981).

[41]S. J. Poon, Phys. Rev. B 25, 1977 (1982).

[42]For a more detailed report see M. G. Karkut, Ph.D. thesis, Indiana University, 1982 (unpublished), available from University Microfilms, P.O. Box 1764, Ann Arbor, Michigan 48106; see also, M. G. Karkut and R. R. Hake, Proceedings of the Fifth International Conference on Liquid and Amorphous Metals, 1983 (in press).

[43]M. G. Karkut and R. R. Hake, Bull. Am. Phys. Soc. 27, 156 (1982).

[44]R. Ray, B. C. Geissen, and N. J. Grant, Scr. Metall. 2, 357 (1968).

[45]R. P. Elliott, in *Constitution of Binary Alloys—First Supplement* (McGraw-Hill, New York, 1965), p. 872.

[46]N. W. Ashcroft and N. D. Mermin, *Solid State Physics* (Holt, Rinehart and Winston, New York, 1976).

[47]Archimedes, On Floating Bodies I. The present adaptation is rather similar to that described by C. Cawthorne and W. D. J. Sinclair, J. Phys. E 5, 531 (1972).

[48]K. A. Gschneidner, Solid State Phys. 16, 275 (1964).

[49]W. B. Pearson, *The Crystal Chemistry and Physics of Metals and Alloys* (Wiley-Interscience, New York, 1972), p. 145.

[50]H. H. Liebermann and C. D. Graham, IEEE Trans. Magn. 12, 921 (1976).

[51]H. H. Liebermann, in *Rapidly Quenched Metals III,* edited by B. Cantor (The Metals Society, London, 1978), Vol. 1, p. 34.

[52]C. A. Pampillo, J. Mater. Sci. 10, 1194 (1975), see Fig. 5.

[53]Allied Chemical Co. data sheets, 1980.

[54]For a discussion, see, e.g., B. D. Cullity, *Elements of X-ray Diffraction* (Addison-Wesley, Reading, 1978), p. 188.

[55]Ö. Rapp, M. Flodin, Å. Östlund, and H. Fredriksson, Phys. Scr. 25, 804 (1982).

[56]Ö. Rapp, M. Flodin, and L. Hedman, in *Superconductivity in d- and f-Band Metals—1982*, Ref. 30, p. 351.

[57]R. R. Hake, M. G. Karkut, and S. Aryainejad, Solid State Commun. 35, 709 (1980).

[58]See, e.g., G. S. Cargill, in *Solid State Physics*, edited by H. Ehrenreich, F. Seitz, and D. Turnbull (Academic, New York, 1975), Vol. 30, p. 227.

[59]W. L. Johnson and A. R. Williams, Phys. Rev. B 20, 1640 (1979).

[60]Y. D. Dong, G. Gregan, and M. G. Scott, J. Non-Cryst. Solids 43, 403 (1981).

[61]Y. Waseda and H. S. Chen, in *Rapidly Quenched Metals III*, edited by B. Cantor (The Metals Society, London, 1978), Vol. 2, p. 415.

[62]Not to be confused with the more commonly known Vegard's law (linear variation of the alloy *lattice parameter* between those of the two alloy constituents). For a discussion of the general failure of both laws in crystalline alloys see Ref. 49, p. 174.

[63]For the most part, calculations utilize standard weak-coupling, dirty-limit relationships given in Ref. 39.

[64]For a recent discussion of high metallic resistivity, see Z. Fisk and G. W. Webb, in *Treatise on Materials Science and Technology: Electronic Structure and Properties*, edited by F. Y. Fradin (Academic, New York, 1981), Vol. 21, p. 297; see also Ref. 65.

[65]P. J. Cote and L. V. Meisel, in *Glassy Metals I*, Ref. 2, p. 141.

[66]R. R. Hake, D. H. Leslie, and T. G. Berlincourt, J. Phys. Chem. Solids 20, 177 (1961).

[67]E. Babić, R. Ristić, M. Miljak, M. G. Scott, and G. Gregan, Solid State Commun. 39, 139 (1981).

[68]K. H. J. Buschow and N. M. Beekmans, Phys. Rev. B 19, 3843 (1979).

[69]Ö. Rapp, B. Lindberg, H. S. Chen, and K. V. Rao, J. Less-Common Met. 62, 221 (1978).

[70]J. A. Rayne and R. A. Levy, in *Amorphous Magnetism II*, edited by R. A. Levy and R. Hasegawa (Plenum, New York, 1977), p. 319.

[71]R. R. Hake, Phys. Rev. Lett. 19, 1105 (1969); J. Appl. Phys. 40, 5148 (1969).

[72]G. Bergmann, Z. Phys. 225, 430 (1969).

[73]Likewise, fluctuation and/or remnant superconductivity usually combine with the normal-state negative-field coefficient of resistivity (negative magnetoresistance) to produce an isothermal peak in $\rho(H, T < 2T_c)$ at about $2H_{c2}(T=0)$, see, e.g., Refs. 33—36 and 74.

[74]J. W. Lue, A. G. Montgomery, and R. R. Hake, Phys. Rev. B 11, 3393 (1975).

[75]R. R. Hake, A. G. Montgomery, and J. W. Lue, in *Low Temperature Physics—LT14*, edited by M. Krusius and M. Vuorio (North-Holland, Amsterdam, 1975), p. 122.

[76]R. R. Hake, Bull. Am. Phys. Soc. 11, 480 (1966); 14, 1176 (1969).

[77]R. R. Hake, in *Proceedings of the Tenth International Low Temperature Conference, Moscow, 1966*, edited by M. P. Malkov (Viniti, Moscow, 1967), Vol. IIa, p. 480.

[78]R. R. Hake, Physica (Utrecht) 55, 344 (1971).

[79]D. Saint-James and P. G. de Gennes, Phys. Lett. 7, 306 (1963).

[80]S. Ami and K. Maki, Phys. Rev. B 18, 4714 (1978).

[81]R. F. Hassing, R. R. Hake, and L. J. Barnes, Phys. Rev. Lett. 30, 6 (1973); 30, 305(E) (1973); S. Ami and K. Maki, Phys. Rev. B 19, 1403 (1979).

[82]P. H. Kes and C. C. Tsuei, Phys. Rev. Lett. 47, 1930 (1981).

[83]R. R. Hake, in *Low Temperature Physics—LT13*, edited by K. D. Timmerhaus, W. J. O'Sullivan, and E. F. Hammel (Plenum, New York, 1974), p. 638.

[84]See references given in Ref. 83 and also Ref. 80.

[85]See, e.g., A. M. Campbell and J. E. Evetts, Adv. Phys. 21, 199 (1972).

[86]B. Abeles, in *Applied Solid State Science* (Academic, New York, 1976), Vol. 6, p. 1.

[87]P. M. Horn and R. D. Parks, Phys. Rev. B 4, 2178 (1971); R. D. Parks (private communication).

[88]J. K. Ekin, Phys. Rev. B 12, 2676 (1975).

[89]N. Toyota, T. Fukase, A. Inoue, Y. Takahashi, and T. Masumoto, Physica 107B, 465 (1981).

[90]R. A. French, J. Lowell, and K. Mendelssohn, Cryogenics 7, 83 (1967).

[91]C. C. Koch, J. O. Scarbrough, D. M. Kroeger, and A. Das Gupta, Appl. Phys. Lett. 37, 451 (1980).

[92]B. M. Clemens, W. L. Johnson, and J. Bennett, J. Appl. Phys. 51, 1116 (1980).

[93]R. R. Hake (unpublished).

[94]A. C. Anderson, C. C. Koch, and J. O. Scarbrough, Phys. Rev. B 26, 1156 (1982).

[95]A. F. Hebard and A. T. Fiory, Physica 109&110B, 1637 (1982).

[96]J. Lowell and A. C. Rose-Innes, Rep. Prog. Phys. 42, 1338 (1979); R. P. Huebener, *Magnetic Flux Structures in Superconductors* (Springer, New York, 1979); J. R. Clem, Phys. Rep. 75, 1 (1981).

[97]M. R. Beasley and C. J. Kircher, in *Superconductor Materials Science*, edited by S. Foner and B. B. Schwartz (Plenum, New York, 1981), p. 605.

[98]See, e.g., Fig. 7 of Y. B. Kim and M. J. Stephen, in *Superconductivity*, edited by R. D. Parks (Dekker, New York, 1969), Vol. 2, p. 1107.

[99]See, e.g., A. I. Larkin and Yu. N. Ovchinnikov, J. Low Temp. Phys. 39, 409 (1979); T. G. Berlincourt, R. R. Hake, and D. H. Leslie, Phys. Rev. Lett. 6, 671 (1961).

[100]For a recent review of experiment and theory, see R. R. Hake, Encyclopedia of Materials Science and Engineering (Pergamon, London, in press).

[101]J. Bardeen, L. N. Cooper, and J. R. Schrieffer, Phys. Rev. 108, 1175 (1957).

[102]W. L. McMillan, Phys. Rev. 167, 331 (1968). For a more recent discussion see, e.g., P. B. Allen, in *Dynami-*

cal Properties of Solids, edited by G. K. Horton and A. A. Maradudin (North-Holland, Amsterdam, 1980), Vol. 3, p. 95; G. Grimvall, *The Electron-Phonon Interaction in Metals* (North-Holland, Amsterdam, 1981); W. B. Butler, in *Treatise on Materials and Science Technology: Electronic Structure and Properties*, Ref. 64, p. 165; C. M. Varma, in *Superconductivity in d- and f-Band Metals—1982*, Ref. 30, p. 603. (Varma thinks the common approximation $\mu^* = 0.13$ for transition metals should be discouraged.)

[103]A. L. Fetter and P. C. Hohenberg, in *Superconductivity*, Ref. 98, esp. 881ff.

[104]T. P. Orlando, E. J. McNiff, S. Foner, and M. R. Beasley, Phys. Rev. B **19**, 4545 (1979); T. P. Orlando and M. R. Beasley, Phys. Rev. Lett. **46**, 1598 (1981); M. R. Beasley, *Advances in Cryogenic Engineering Materials* (Plenum, New York, 1982), Vol. 28, p. 345; T. P. Orlando, in *Superconductivity in d- and f-Band Materials—1982*, Ref. 30, p. 75. Recent calculations by W. Hänsch (unpublished) suggest that the Orlando-Beasley-Rainer method of grafting phonon renormalization corrections onto the WHHM theory is correct.

[105]M. Ikebe, Y. Muto, S. Ikeda, H. Fujimori, and K. Suzuki, Physica **107B**, 387 (1981).

[106]O. Bethoux, O. Laborde, L. C. Lasjaunias, and A. Ravex, J. Phys. (Paris) Colloq. **41**, C8-754 (1980).

[107]D. Rainer, G. Bergmann, and U. Eckhardt, Phys. Rev. B **8**, 5324 (1973).

[108]N. Schopohl and K. Scharnberg, Physica **107B**, 293 (1981).

[109]G. Bergmann, Phys. Rev. B **7**, 4850 (1973). This formula is equivalent to $\gamma_v = \alpha/(2.35\rho_n)$ of Ref. 39 with units as specified therein, and may be derived from Abrikosov's $H_{c2} = \sqrt{2}\kappa H_c$, Gor'kov's dirty limit

$$\kappa \approx \kappa_l = ec\gamma_v^{1/2}\rho_n(k_B\pi^3)^{-1}[21\zeta(3)/2\pi]^{1/2},$$

and the weak coupling BCS $(dH_c/dT)^2_{T_c}$ $= (4\pi/T_c)(\Delta C)_{T_c}$ where the jump in the zero-H specific heat at T_c, $\Delta C = 1.43\gamma_v T_c$ (see, e.g., Ref. 39).

[110]D. E. Moody and T. G. Ng, in *Proceedings of the International Conference on the Physics of Transition Metals, 1980*, edited by P. Rhodes (IOP, London, 1981), p. 631.

[111]A. Ravex, J. C. Lasjaunias, and O. Bethoux, Solid State Commun. **40**, 853 (1981).

[112]P. Oelhafen, E. Hauser, H.-J. Güntherodt, and K. H. Bennemann, Phys. Rev. Lett. **43**, 1134 (1979).

[113]A. Amamou and G. Krill, Solid State Commun. **28**, 957 (1978).

[114]P. Oelhafen, E. Hauser, and H-J. Güntherodt, Solid State Commun. **35**, 1017 (1980).

[115]A. Amamou, Solid State Commun. **37**, 7 (1980).

[116]A. Amamou, Solid State Commun. **33**, 1029 (1980).

[117]For a discussion, see Ref. 65.

[118]R. S. Nagel and J. Tauc, Phys. Rev. Lett. **35**, 380 (1976).

[119]A. B. Pippard, Rev. Mod. Phys. **36**, 328 (1964).

[120]J. D. Meyer, F. Ochmann, and B. Stritzker, Solid State Commun. **39**, 419 (1981). Extrapolation of these data suggests $T_c \approx 1.5$ K for pure amorphous Zr, less than the $T_c \approx 3.5$ K suggested by the measurements of Ref. 9. The high ρ_n and negative-temperature coefficient of resistivity reported for $Ti_{87}Fe_{13}$ by Meyer *et al.* do not necessarily imply amorphism since similar behavior is observed in crystalline TiFe alloys; J. W. Lue, A. G. Montgomery, and R. R. Hake, in *Magnetism and Magnetic Materials—1974 (San Francisco)*, Proceedings of the 20th Annual Conference on Magnetism and Magnetic Materials, edited by C. D. Graham, Jr., G. H. Lander, and J. J. Rhyne (AIP, New York, 1975), p. 432.

[121]W. L. Johnson, in *Superconductivity in d- and f-Band Materials—1982*, Ref. 30, p. 341.

[122]G. R. Gruzalski, J. A. Gerber, and D. J. Sellmyer, Phys. Rev. B **19**, 3469 (1979).

[123]S. J. Poon and W. L. Carter, Solid State Commun. **35**, 249 (1980).

[124]B. T. Matthias, in *Progress in Low Temperature Physics*, edited by C. J. Gorter (North-Holland, Amsterdam, 1957), Vol. II, p. 138.

[125]E. Bucher, F. Heiniger, J. Muheim, and J. Muller, Rev. Mod. Phys. **36**, 146 (1964).

[126]W. L. Johnson and S. J. Poon, J. Appl. Phys. **46**, 1787 (1975).

[127]K. H. J. Buschow, J. Magn. Magn. Mater. **28**, 20 (1982).

[128]D. Pines, Phys. Rev. **109**, 280 (1958); R. R. Hake, *ibid.* **123**, 1986 (1961).

[129]J. K. Hulm and R. D. Blaugher, in *Superconductivity in d- and f-Band Metals—1971 (Rochester)*, Proceedings of the Conference on Superconductivity in d- and f-Band Metals, edited by D. H. Douglas (AIP, New York, 1972), p. 1.

[130]C. M. Varma and R. C. Dynes, in *Superconductivity in d- and f-Band Metals*, edited by D. H. Douglas (Plenum, New York, 1976), p. 507.

[131]W. H. Butler, Phys. Rev. B **15**, 5267 (1977); see also Ref. 64, p. 165.

[132]J. Willer, G. Fritsch, and E. Lüscher, J. Less-Common Met. **77**, 191 (1981).

[133]J. A. Cape and R. R. Hake, Phys. Rev. **139**, A142 (1965); H. C. Jones, A. G. Montgomery, I. B. Lin, J. W. Lue, H. Nadler, and R. R. Hake, Phys. Rev. B **16**, 1177 (1977).

[134]R. C. Dynes and C. M. Varma, J. Phys. F **6**, L215 (1976).

[135]K. H. Bennemann, *Liquid and Amorphous Metals*, Ref. 7, p. 253.

[136]See, e.g., Fig. 4.4, p. 156 of Ref. 49, or Fig. 11, p. 322 of Ref. 48.